Geophys. J. Int. (2007) doi: 10.1111/j.1365-246X.2007.03527.x

Guided waves in marine CSEM

Peter Weidelt

Institut für Geophysik und Extraterrestrische Physik, Technische Universität Braunschweig, D-38106 *Braunschweig, Germany. E-mail: p.weidelt@tu-bs.de*

Accepted 2007 June 18. Received 2007 June 18; in original form 2006 December 22

SUMMARY

Recently, marine controlled source electromagnetics (CSEM) has shown great potential in hydrocarbon exploration, where the goal is to detect thin resistive layers at depth below the seafloor. The experiment comprises a horizontal electric dipole transmitter towed over an array of receivers at the seafloor. The transmitter emits a low-frequency signal (<1 Hz) and measurements of the electric field are made. The depth of the target layer requires transmitter–receiver separations of several kilometres. As a function of separation r, the electromagnetic signal consists of a short-ranging contribution with an exponential decay resulting from the transmission through ocean and sediment (including the reflection at all interfaces) and a long-ranging contribution with a dominant $1/r^3$-decay associated with the airwave guided at the air–ocean interface. Of particular interest among the exponentially decaying waves is the wave guided in the resistive target layer with a well-defined long decay length. In a shallow sea, this 'resistive-layer mode' is partly masked by the airwave.

The topics of this study are the airwave and the resistive-layer mode. For a general 1-D conductivity distribution we derive the simple expression of the leading term of the airwave for arbitrary transmitter and receiver position and define a 'pure' complete airwave, which for all separations is close to the asymptotic expansion of the airwave in powers of $1/r$. Whereas the treatment of the airwave can be done in terms of Bessel function integrals with real wavenumbers, the resistive-layer mode requires the complex wavenumber plane, where it is defined as the residual at the TM-mode pole with the smallest imaginary part. For sufficiently high integrated resistivity of the layer, we give a simple method to determine the position of this pole. In the complex wavenumber plane, the pure complete airwave is presented by a branch-cut integral. For a typical model, this study concludes with the remarkable result that the superposition of airwave and resistive-layer mode provides an excellent description of the electric field over a wide range of separations.

Key words: electrical conductivity, electromagnetic induction, guided waves, layered media, oceans, wave propagation.

1 INTRODUCTION

The recent success of marine controlled source electromagnetics (CSEM) in off-shore hydrocarbon exploration (Eidsmo *et al.* 2002; Ellingsrud *et al.* 2002) has renewed the interest in this method, which has been used since the 1980s for studies of the oceanic lithosphere (e.g. Cox 1980; Chave *et al.* 1991). In the marine CSEM exploration method, an electric dipole with a transient or low-frequency continuous wave excitation is towed over an array of seafloor receivers that measure the electric and/or magnetic field (e.g. Edwards 2005). The targets are typically thin sedimentary layers that are resistive because they are saturated with hydrocarbons. In view of the variety of different experimental setups, the data type considered in this study is restricted by focusing on continuous wave excitation (with a typical frequency of 0.5 Hz) and on electric fields.

Using continuous wave excitation, the target depths of up to 1000 m below the seafloor require transmitter–receiver separations of several kilometres. The electromagnetic skin effect in the sea and seafloor sediments dominates at short separations and leads, both for the direct signal and the signal reflected at interfaces, to an exponential decay with a horizontal decay length of approximately 630 m (combined effect of sea and seafloor sediments at 0.5 Hz). For greater separations, the measured signal is influenced by the insulating air half-space and, if present, also by the resistive target layer. In the insulating air, with its infinite depth of penetration and vertical extent, the horizontal decay of the signal is purely geometrical and all electromagnetic field components (except the vertical electric field) decay as $1/r^3$, where r is the horizontal separation between source and receiver. By the continuity of the tangential electromagnetic field across the air–ocean interface, this asymptotic $1/r^3$-behaviour is imparted onto the electromagnetic field inside the earth, which then shows the same asymptotic

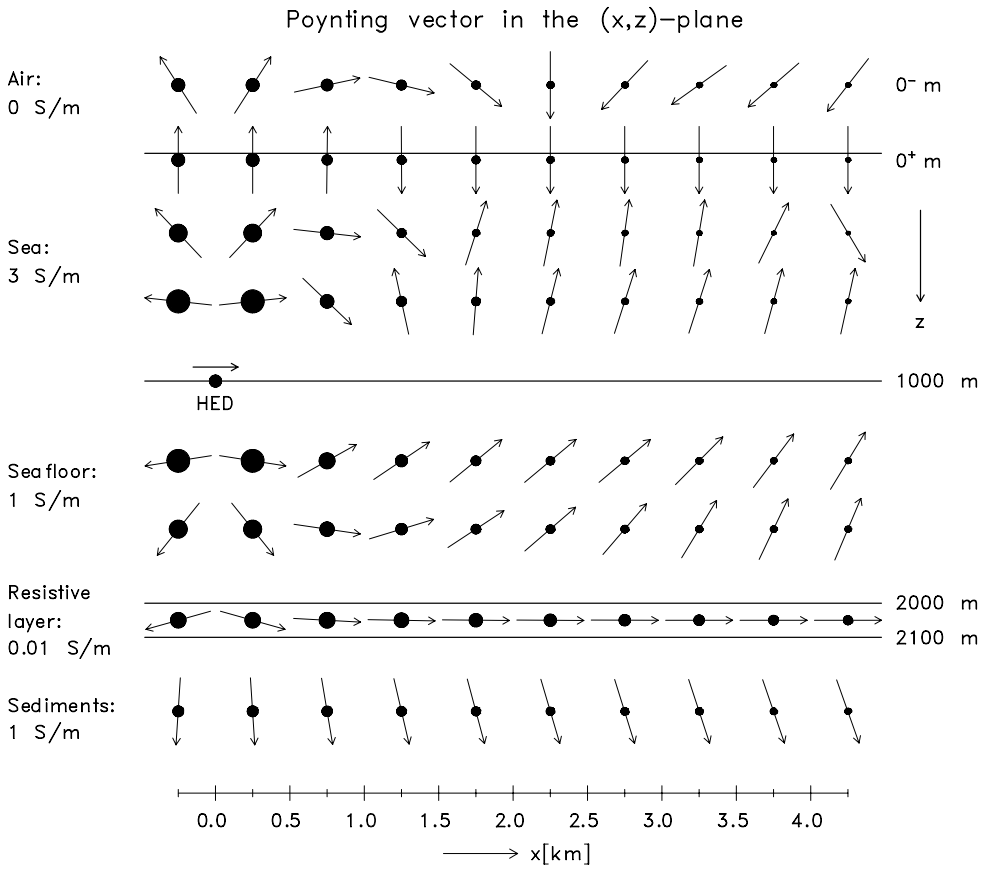

Figure 1. Time-harmonic horizontal electric dipole in x-direction at $x_0 = y_0 = 0$ and $z_0 = 1000$ m with $f = 0.5$ Hz. The conductivity model shown (the 'standard model') and the frequency will be used throughout in this study. The time-averaged energy flow is displayed in the (x, z)-plane at $y = 0$ by means of the Poynting vector $\overline{\mathbf{S}}$. The arrows show only the direction of $\overline{\mathbf{S}}$, the strength $|\overline{\mathbf{S}}|$ with its great dynamic range is presented by the size of the black circles, such that an increase of the diameter by a factor of 2 corresponds to an increase of $|\overline{\mathbf{S}}|$ by a factor of 1000. The discontinuity of E_z at $z = 0$ introduces a discontinuity in $\overline{S}_x$. Therefore, the arrows for $z = 0^-$ are drawn for clarity with a vertical displacement.

behaviour. This contribution is called the 'airwave' (e.g. Constable & Weiss 2006). Also, the resistive layer gives rise to a long-ranging far-field contribution. Its small positive conductivity leads to an exponential far-field decay with a well-defined decay length, mainly determined by the local penetration depth, but decreased by non-linear interaction with adjacent conductors. For the standard conductivity model considered in this study (see Figs 1 and 2), the decay length is on the order of 1700 m. This resistive layer contribution to the far-field is the 'resistive-layer mode'. Mathematically, it is the residual of a particular pole in the complex wavenumber domain.

This study shows that electromagnetic seafloor data contain, in addition to short-ranging contributions controlled by the local penetration depth, long-ranging contributions resulting from remote resistive structures such as the insulating air half-space and the resistive layer. These contributions are 'guided waves', where the air–ocean interface and the resistive layer serve as 'wave guides'. Although from the same physical origin, the following discussion reveals that the two guided waves are actually quite different.

A useful concept of controlled source electromagnetic induction in a layered earth is the decomposition of the electromagnetic field into a TE-mode (= tangential electric, i.e. vertical electric field missing) and a TM-mode (= tangential magnetic, i.e. vertical magnetic field missing). These modes propagate without coupling through a layered structure, and are coupled only through the source, which generally excites both modes. In the TE-mode, electromagnetic coupling between adjacent layers is inductive. Therefore, a very thin resistive (or even insulating) layer has virtually no influence on the progation of this mode. In the TM-mode, adjacent layers are coupled galvanically. Thus a very thin resistive layer acts as an efficient barrier shielding deeper conductors from the TM-mode. Thus the resistive-layer mode with its well-defined exponential decay length is a pure TM-mode phenomenon.

Whereas the TE-mode bridges an insulating layer of finite thickness by inductive coupling to a conducting half-space in the direction of propagation, the infinite insulating air half-space cannot be bridged. Due to the continuity of the tangential electromagnetic field across the interfaces, the geometrical $1/r^3$-decay is imparted onto the field inside the earth. The TM-mode inside the conductor decays exponentially and, therefore, plays no role in the formation of the airwave. The airwave is a pure TE-mode phenomenon. Therefore, it is present also in controlled source setups requiring only the TE-mode, for example in vertical magnetic dipole sources or horizontal line currents. (For the latter, the decay is only $\sim 1/r^2$.) Particularly in subsurface to subsurface communication, the airwave is also called a 'lateral wave' (e.g. Bannister 1984; King *et al.* 1992).

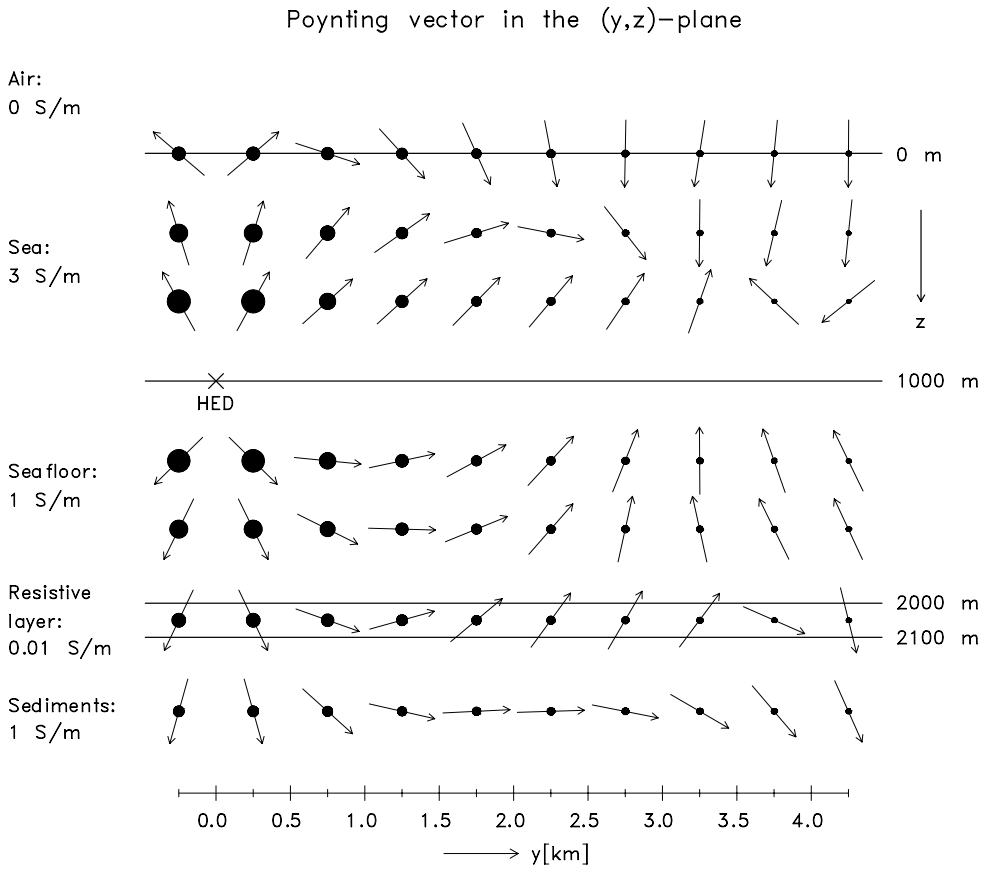

Figure 2. The same model as in Fig. 1. Now the Poynting vector $\overline{\mathbf{S}}$ is displayed in the (y, z)-plane at $x = 0$.

Finally, we attempt to visualize the energy flow in marine CSEM using a low-frequency horizontal electric dipole (HED) source. Since in the frequency domain the electromagnetic field is governed by a Helmholtz equation (elliptic) rather than by a diffusion equation (parabolic) or a wave equation (hyperbolic), we cannot visualize the energy flow by rays. See also the discussion by Løseth *et al.* (2006). Instead we use a presentation in terms of the time-averaged real Poynting vector (e.g. Stratton 1941, p. 137 or Jackson 1975, p. 241)

$$\overline{\mathbf{S}} := \frac{1}{2\mu_0}\mathrm{Re}(\mathbf{E} \times \mathbf{B}^*), \tag{1}$$

where $\mathbf{E}$ and $\mathbf{B}$ are the complex electric and magnetic field vectors and * denotes the complex conjugate. Only the integral of the normal component of $\overline{\mathbf{S}}$ over a closed surface has a definite physical meaning as energy dissipated per unit time in the enclosed volume. The local interpretation of $\overline{\mathbf{S}}$ as energy flow density at a point is not without problems (Jones 1964, p. 52), since one has the freedom to add a non-divergent vector to $\overline{\mathbf{S}}$. With this caveat in mind, the display of $\overline{\mathbf{S}}$ will at least provide some idea about the energy flow.

For an embedded HED in x-direction at $x_0 = y_0 = 0$ the vector $\overline{\mathbf{S}}$ is presented on two orthogonal cross-sections through the dipole. Fig. 1 shows $\overline{\mathbf{S}}$ in the (x, z)-plane at $y = 0$ with the components

$$\overline{S}_x = -\frac{1}{2\mu_0}\mathrm{Re}\big(E_z B_y^*\big), \quad \overline{S}_z = +\frac{1}{2\mu_0}\mathrm{Re}\big(E_x B_y^*\big), \tag{2}$$

whereas Fig. 2 displays $\overline{\mathbf{S}}$ in the (y, z)-plane at $x = 0$ with the components

$$\overline{S}_y = -\frac{1}{2\mu_0}\mathrm{Re}\big(E_x B_z^*\big), \quad \overline{S}_z = +\frac{1}{2\mu_0}\mathrm{Re}\big(E_x B_y^*\big). \tag{3}$$

The arrows of unit length show the direction of $\overline{\mathbf{S}}$, its strength is indicated by the size of the black circles (see the caption to Fig. 1 for details). In the cross-sections shown, the components $\overline{S}_y$ and $\overline{S}_z$ are continuous across layer boundaries, whereas the discontinuity in E_z introduces a discontinuity in $\overline{S}_x$. Most evident is the different expression of the resistive layer. In the (x, z)-plane with its galvanic coupling, the strong values of E_z produce an enhanced energy flow in x-direction with only little dissipation (Fig. 1). In the (y, z)-plane (Fig. 2), the resistive layer is bridged by inductive coupling and remains invisible.

The airwave is seen in both cross-sections. It consists of an upward transport of energy by E_x and B_y and, at greater separations, of a downward transport by the same components. The horizontal energy transport is organized in the (x, z)-plane by E_z and B_y and in the in the (y, z)-plane by E_x and B_z. These observations show that the local interpretation of $\overline{\mathbf{S}}$ as energy flow density leads to results expected from

physical intuition. A different attempt to visualize the pertinent CSEM fields at low-frequency induction has been undertaken by Um & Alumbaugh (2007), who present an extensive collection of current density plots.

The paper is organized as follows. As the starting point of this study, Section 2 gives a concise general representation of the electromagnetic field of a HED embedded in a layered conductor. Section 3 is devoted to the airwave. It includes the derivation of the leading term of the airwave for a general 1-D conductivity distribution and for general positions of source and receiver. Moreover, we propose different completions of the airwave, which reproduce all asymptotic terms. Finally, Section 4 generalizes the usual Hankel transform representations of the field components to contours in the complex wavenumber domain, in which the guided waves can be identified as particular singularities: the complete airwave as a branch cut and the resistive-layer mode as a pole. Most of the mathematical details are given in the appendices.

2 BASIC PRESENTATIONS

In a layered 1-D medium of conductivity $\sigma(z)$ and vacuum magnetic permeability μ_0 the electromagnetic field admits a decomposition into a TE-mode (subscript e) and a TM-mode (subscript m) as

$$\mathbf{B} = \mathbf{B}_e + \mathbf{B}_m = \nabla \times \nabla \times (\hat{\mathbf{z}}\chi_e) + \nabla \times (\hat{\mathbf{z}}\chi_m), \tag{4}$$

$$\mathbf{E} = \mathbf{E}_e + \mathbf{E}_m = -i\omega\nabla \times (\hat{\mathbf{z}}\chi_e) + 1/(\mu_0\sigma)\nabla \times \nabla \times (\hat{\mathbf{z}}\chi_m), \tag{5}$$

(e.g. Chave & Cox 1982). The time factor is $e^{+i\omega t}$, $\omega > 0$. Used are cylindrical coordinates (r, φ, z) with z positive downwards and the air–ocean interface at $z = 0$. Moreover, the horizontal Cartesian coordinates are given by $x = r\cos\varphi$, $y = r\sin\varphi$. A HED with current moment $\mathbf{p} = p\hat{\mathbf{x}}$ is placed at $r = 0$, $z = z_0 \geq 0$. The position of the receiver is given by the vector $\mathbf{r} = r\hat{\mathbf{r}} + \varphi\hat{\boldsymbol{\varphi}} + z\hat{\mathbf{z}}$. Then the TE-mode potential $\chi_e(\mathbf{r})$ is

$$\chi_e(\mathbf{r}) = \frac{\mu_0 p}{2\pi}\int_0^\infty \frac{f_{eb}(z)/f_{eb}(z_0)}{a_e(z_0)+b_e(z_0)}\,J_1(\kappa r)\,\mathrm{d}\kappa\,\sin\varphi, \quad z \geq z_0, \tag{6}$$

$$\chi_e(\mathbf{r}) = \frac{\mu_0 p}{2\pi}\int_0^\infty \frac{f_{ea}(z)/f_{ea}(z_0)}{a_e(z_0)+b_e(z_0)}\,J_1(\kappa r)\,\mathrm{d}\kappa\,\sin\varphi, \quad z \leq z_0 \tag{7}$$

and the TM-mode potential $\chi_m(\mathbf{r})$ reads

$$\chi_m(\mathbf{r}) = +\frac{\mu_0 p}{2\pi}\int_0^\infty \frac{a_m(z_0)f_{mb}(z)/f_{mb}(z_0)}{a_m(z_0)+b_m(z_0)}\,J_1(\kappa r)\,\mathrm{d}\kappa\,\cos\varphi, \quad z > z_0, \tag{8}$$

$$\chi_m(\mathbf{r}) = -\frac{\mu_0 p}{2\pi}\int_0^\infty \frac{b_m(z_0)f_{ma}(z)/f_{ma}(z_0)}{a_m(z_0)+b_m(z_0)}\,J_1(\kappa r)\,\mathrm{d}\kappa\,\cos\varphi, \quad z < z_0. \tag{9}$$

For ease of notation, the additional dependence of $a_{e,m}$, $b_{e,m}$, $f_{ea,b}$ and $f_{ma,b}$ on κ has been suppressed. The TE-mode functions $f_e(z) := f_{ea}(z)$ and $f_e(z) := f_{eb}(z)$ are solutions of the ordinary differential equation

$$f_e''(z) = \alpha^2(z) f_e(z), \quad \alpha^2(z) := \kappa^2 + i\omega\mu_0\sigma(z), \tag{10}$$

vanishing, respectively, for $z \to -\infty$ (upward propagation) and for $z \to +\infty$ (downward propagation). At conductivity discontinuities f_e and f_e' are continuous. From $f_{ea}(z)$ and $f_{eb}(z)$ we derive the (continuous) transfer functions

$$a_e(z) := +f_{ea}'(z)/f_{ea}(z) \quad \text{and} \quad b_e(z) := -f_{eb}'(z)/f_{eb}(z). \tag{11}$$

Physically, $i\omega\mu_0/a_e$ and $i\omega\mu_0/b_e$ are the TE-mode spectral impedances of the upgoing and downgoing wave. Similarly, the TM-mode functions $f_m(z) := f_{ma}(z)$ and $f_m(z) := f_{mb}(z)$ are solutions of the ordinary differential equation

$$\sigma(z)[f_m'(z)/\sigma(z)]' = \alpha^2(z) f_m(z), \tag{12}$$

vanishing, respectively, for $z \to -\infty$ and for $z \to +\infty$. At conductivity discontinuities f_m and f_m'/σ are continuous. From $f_{ma}(z)$ and $f_{mb}(z)$ the (continuous) transfer functions are

$$a_m(z) := +f_{ma}'(z)/[\sigma(z) f_{ma}(z)] \quad \text{and} \quad b_m(z) := -f_{mb}'(z)/[\sigma(z) f_{mb}(z)], \tag{13}$$

where a_m and b_m are the TM-mode spectral impedances. For real wavenumber κ, the transfer functions $a_{e,m}$ and $b_{e,m}$ are in the first quadrant of the complex plane, see eqs (73)–(76) in Section 4.1.

From eq. (5) the horizontal electric field components are given by

$$E_r = -(i\omega/r)\partial_\varphi\chi_e + 1/(\mu_0\sigma)\partial_{rz}^2\chi_m, \quad E_\varphi = i\omega\partial_r\chi_e + 1/(r\mu_0\sigma)\partial_{\varphi z}^2\chi_m \tag{14}$$

or explicitly

$$E_r(\mathbf{r}) = -\frac{i\omega\mu_0 p}{2\pi}\int_0^\infty [Q_e(z\,|\,z_0,\kappa)\,(1/r) + Q_m(z\,|\,z_0,\kappa)\,\partial_r]J_1(\kappa r)\,\mathrm{d}\kappa\,\cos\varphi, \tag{15}$$

$$E_\varphi(\mathbf{r}) = +\frac{i\omega\mu_0 p}{2\pi}\int_0^\infty [Q_e(z\,|\,z_0,\kappa)\,\partial_r + Q_m(z\,|\,z_0,\kappa)\,(1/r)]J_1(\kappa r)\,\mathrm{d}\kappa\,\sin\varphi \tag{16}$$

with (suppressing again the argument κ)

$$Q_e(z\,|\,z_0) := \frac{f_{eb}(z)/f_{eb}(z_0)}{a_e(z_0)+b_e(z_0)}, \quad z \geq z_0, \tag{17}$$

$$Q_m(z\,|\,z_0) := \frac{1}{i\omega\mu_0}\,\frac{a_m(z_0)\,b_m(z)}{a_m(z_0)+b_m(z_0)}\,\frac{f_{mb}(z)}{f_{mb}(z_0)}, \quad z \geq z_0. \tag{18}$$

For $z < z_0$ retain all arguments, but replace f_{eb} by f_{ea} in eq. (17) and f_{mb} by f_{ma} in eq. (18). Moreover, interchange a_m and b_m in the numerator of eq. (18).

Q_e and Q_m are continuous with respect to z and z_0 and satisfy the reciprocity relations

$$Q_e(z\,|\,z_0) = Q_e(z_0\,|\,z), \quad Q_m(z\,|\,z_0) = Q_m(z_0\,|\,z). \tag{19}$$

These relations are easily proved by inserting eqs (11) and (13) into eqs (17) and (18) and exploiting the fact that the Wronskians

$$W_e(z) := f_{eb}(z)f'_{ea}(z) - f_{ea}(z)f'_{eb}(z), \tag{20}$$

and

$$W_m(z) := [f_{mb}(z)f'_{ma}(z) - f_{ma}(z)f'_{mb}(z)]/\sigma(z), \tag{21}$$

do not depend on z. This property of the Wronskians, which is used extensively in the present study, is verified by showing that the differential eqs (10) and (12) imply $W'_{e,m}(z) = 0$.

3 THE AIRWAVE

3.1 The leading term in the electric field

In marine CSEM two propagation paths are important. First, there is the transmission through oceans and sediments and the reflection at interfaces (including the air–ocean interface), both of which are associated with an exponential decay with horizontal separation r. Secondly there is the airwave guided at the air–ocean interface, which decays at long distances only $\sim 1/r^3$ and, therefore, is the dominating signal in the far-field. An example for the occurrence of the airwave is shown and explained in Fig. 3. It is related to the 'standard model' of Fig. 1.

This leading term of the airwave with its radial $1/r^3$-decay is easily expressed in terms of the conductivity structure and the position of source and receiver. Assume in $z < 0$ an insulating air half-space and in $z > 0$ the earth/sea with a 1-D conductivity distribution $\sigma(z)$ bounded from below by $\sigma_{\min}$, that is, $\sigma(z) \geq \sigma_{\min} > 0$. Then for arbitrary transmitter depth $z_0 \geq 0$ and arbitrary receiver depth $z \geq 0$, the leading term

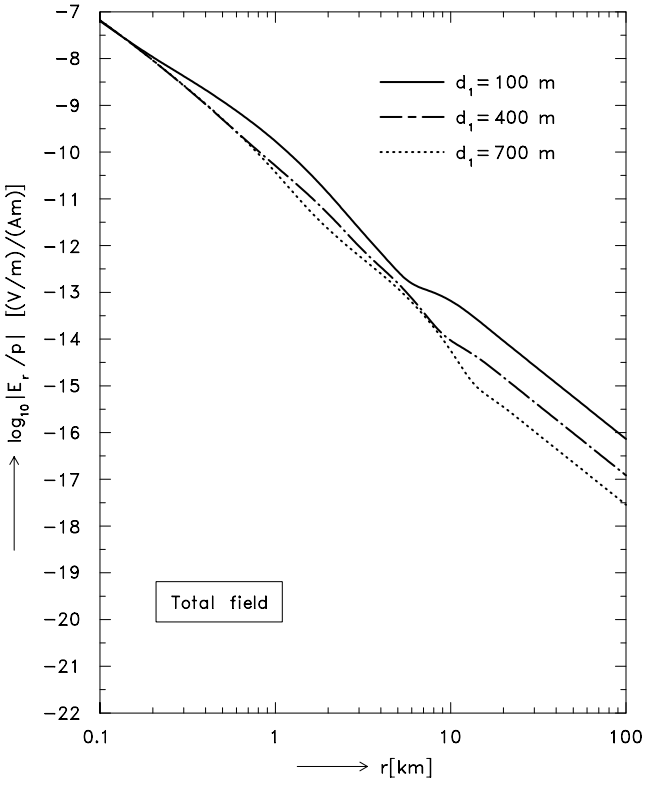

Figure 3. Radial component E_r of the electric field, normalized with the current moment p of the electric dipole for various water depths d_1. Transmitter and receiver in in-line configuration are placed at the ocean bottom, $z = z_0 = d_1$. The conductivity below the ocean follows the model of Fig. 1. The frequency is $f = 0.5$ Hz. In this log–log plot, the leading term of the airwave with its decay $\sim 1/r^3$ is seen in the linear sections of the far-field. At shallow depth ($d_1 = 100$ and 400 m) the airwave masks the signal of the resistive layer, which manifests itself for $d_1 = 700$ m in the curved section between $r \approx 3$ and 10 km.

of the airwave (identified by the subscript 0) admits the representation

$$E_{0r}^{\rm air}(\mathbf{r}) = \frac{i\omega\mu_0\, p\cos\varphi}{2\pi r^3}\,\frac{e(z)\,e(z_0)}{[e'(0)]^2}, \tag{22}$$

$$E_{0\varphi}^{\rm air}(\mathbf{r}) = \frac{i\omega\mu_0\, p\sin\varphi}{\pi r^3}\,\frac{e(z)\,e(z_0)}{[e'(0)]^2}, \tag{23}$$

where $e(z)$ is the downward propagating solution of eq. (10) in the limit $\kappa = 0$, that is, of

$$e''(z) = i\omega\mu_0\sigma(z)\,e(z). \tag{24}$$

Physically, $e(z)$ is the electric field in 1-D magnetotellurics. Because 1-D magnetotellurics is insensitive to thin poor conductors, the resistive target layer is barely seen in the airwave. The reciprocity (19) is reflected in the symmetry of the airwave with respect to z and z_0.

The formally simplest airwave arises in a uniform half-space of conductivity σ. Then $e(z) \sim \mathrm{e}^{-kz}$, $k^2 := i\omega\mu_0\sigma$ and

$$E_{0r}^{\rm air}(\mathbf{r}) = \frac{p\,\mathrm{e}^{-k(z+z_0)}\cos\varphi}{2\pi\sigma r^3}, \quad E_{0\varphi}^{\rm air}(\mathbf{r}) = \frac{p\,\mathrm{e}^{-k(z+z_0)}\sin\varphi}{\pi\sigma r^3}. \tag{25}$$

The amplitude decreases exponentially with increasing depth of transmitter and/or receiver. The result (25) has been given by different authors, for example, by Wait (1961, p. 1026), Bannister (1984, Table 1) and Constable & Weiss (2006, p. G46).

Here we sketch only the major steps leading to the general formulas (22) and (23); details are given in Appendix A. According to eqs (15) and (16) the electric field components E_r and E_φ can be expressed in terms of the Hankel transform

$$g_1(r) := \int_0^\infty f(\kappa)\,J_1(\kappa r)\,\mathrm{d}r \tag{26}$$

and its derivative $g_1'(r)$. Assuming that a Taylor expansion of $f(\kappa)$ at $\kappa = 0$ exists,

$$f(\kappa) = \sum_{n=0}^{\infty}\frac{\kappa^n}{n!}\,f^{(n)}(0), \tag{27}$$

we obtain for $r \to \infty$ the asymptotic formula (Tranter 1966, p. 67)

$$g_1(r) = \frac{f(0)}{r} + \sum_{m=0}^{\infty}\binom{-1/2}{m}\frac{f^{(2m+1)}(0)}{r^{2m+2}}. \tag{28}$$

The Taylor expansion of $f(\kappa)$ at $\kappa = 0$ leads for $g_1(r)$ to an expansion in terms of powers of $1/r$. If it happens that $f(0)$ and all odd derivatives $f^{(2m+1)}(0)$ are vanishing, the transform $g_1(r)$ decays for $r \to \infty$ faster than any power of $1/r$, it decays exponentially. Physically, the exponential decay will describe the transmission through oceans and sediments (including the reflection at all interfaces), whereas the slower decay in powers of $1/r$ is associated with the airwave guided at the air–ocean interface.

First it is proved in Appendix A1 that

$$Q_e(z\,|\,z_0, 0) = Q_m(z\,|\,z_0, 0). \tag{29}$$

As a consequence, a term $\sim 1/r^2$, which is present in the separate asymptotic expansion of the TE- and TM-mode part of E_r and E_φ, will vanish when the total field is considered.

Secondly it is shown in Appendix A2 that, for $\kappa \neq 0$,

$$Q_e(z\,|\,z_0, -\kappa) \neq Q_e(z\,|\,z_0, +\kappa), \quad Q_m(z\,|\,z_0, -\kappa) = Q_m(z\,|\,z_0, +\kappa). \tag{30}$$

Since Q_m is an even function of κ, all odd derivatives at $\kappa = 0$ vanish. Therefore, the TM-mode part of the electric field decays exponentially with separation r and the leading term results only from the TE-mode, as expected. The presentations (15) and (16) in conjunction with the results (28)–(30) yield as leading term

$$E_{0r}^{\rm air}(\mathbf{r}) = -\frac{i\omega\mu_0\, p\cos\varphi}{2\pi r^3}\,\partial_\kappa Q_e(z\,|\,z_0, \kappa)|_{\kappa=0}, \tag{31}$$

$$E_{0\varphi}^{\rm air}(\mathbf{r}) = -\frac{i\omega\mu_0\, p\sin\varphi}{\pi r^3}\,\partial_\kappa Q_e(z\,|\,z_0, \kappa)|_{\kappa=0}. \tag{32}$$

The evaluation of $\partial_\kappa\, Q_e(z|z_0, \kappa)|_{\kappa=0}$ in Appendix A3 then leads to eqs (22) and (23).

Fig. 4 shows the data from Fig. 3 after removing the leading term (22). It is emphasized that this efficient removal was possible only because $\sigma(z)$ was assumed to be known. At great separations r, well below the error floor of the signals, the curves split indicating that the second term in the asymptotic expansion of the airwave, decaying $\sim 1/r^5$, becomes relevant. For details see the caption to Fig. 4.

After treating the leading term of the tangential electric field, we briefly consider the asymptotic behaviour of the vertical component $E_z(\mathbf{r})$. Taking, for instance, $z > z_0 > 0$ and using eqs (5) and (8), this component is given by (see also Appendix A4)

$$E_z(\mathbf{r}) = \frac{p}{2\pi\sigma(z)}\int_0^\infty \frac{\kappa^2 a_m(z_0) f_{mb}(z)/f_{mb}(z_0)}{a_m(z_0) + b_m(z_0)}\,J_1(\kappa r)\,\mathrm{d}\kappa\cos\varphi. \tag{33}$$

Since E_z is a pure TM-mode field, it does not show the airwave effect. Mathematically, it follows from Appendix A2 that the kernel is an even function of κ and, therefore, inside the earth, E_z vanishes exponentially for $r \to \infty$. For the standard model with a shallow sea ($d_1 = 100$ m),

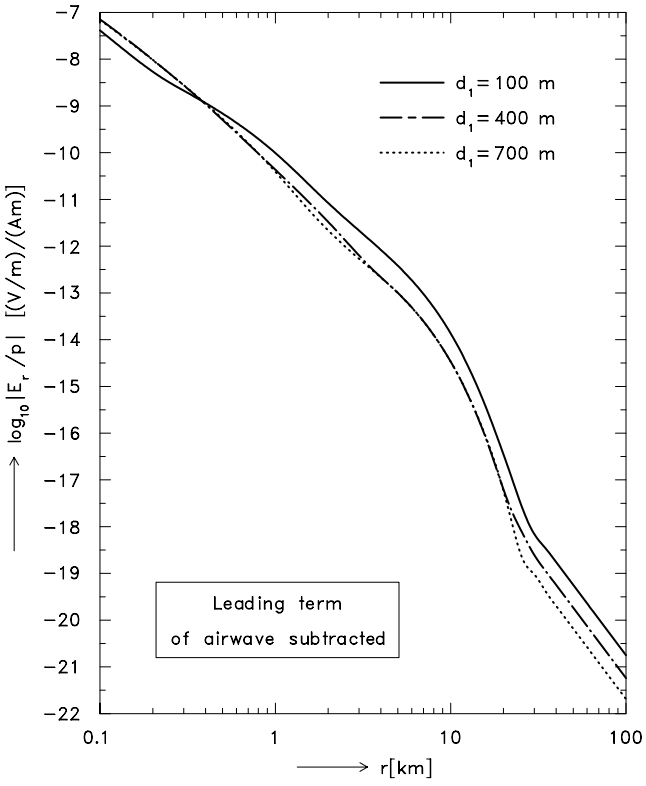

Figure 4. Subtraction of the leading airwave term (22) from the data shown in Fig. 3. The resistive-layer signal now becomes visible for all water depths d_1. The subtraction removes only the far-field with its $1/r^3$-decay. The reflections at the air–ocean interface with an exponential decay, occurring at intermediate separations, are not eliminated. The linear sections, occurring for separations greater than 20 km, have a decay $\sim 1/r^5$ and represent the second asymptotic term of the airwave, which is neglected in eq. (22). Even with an optimistic error floor of 10^{-16} (V/m)/(Am) (Constable & Weiss 2006), this second term will not be seen in the data.

the component E_z is shown in the lower part of Fig. 5 by the solid line. The response for a modified model, in which the conductivity of the target layer (0.01 S m^{-1}) is replaced by the background conductivity (1 S m^{-1}), is displayed by the dotted line. The straightline portions of these graphs indicate the asymptotic exponential decay. The different decay lengths (1750 m in the first model and 700 m in the second) clearly discriminate between these models, if E_z could be measured with the required accuracy. Unfortunately, this is not yet the case. The two graphs in the upper part of Fig. 5 show the corresponding radial component E_r. This component is dominated by the airwave, which is insensitive to the resistive layer.

The discontinuous component E_z, with $E_z \equiv 0$ at the sea-side $z = 0^+$ of the air–ocean interface, is strongly guided at the atmospheric side $z = 0^-$, where it decays for $r \to \infty$ only $\sim 1/r^2$,

$$E_z(r, \varphi, 0^-) \approx \frac{i\omega\mu_0 p \cos\varphi}{2\pi r^2} \frac{e(z_0)}{e'(0)}. \tag{34}$$

Again $e(z)$ is a downward propagating solution of eq. (24). The derivation of this result is briefly sketched in Appendix A4.

3.2 The leading airwave term in the magnetic field

The airwave is also present in the TE-mode part of the magnetic field. This warrants a brief look into the leading term of the field components. According to eq. (5) we have $\mathbf{E}_0^{\text{air}} = -i\omega\nabla \times (\hat{\mathbf{z}}\chi_e)$. Comparison with eqs (22) and (23) yields

$$\chi_e(\mathbf{r}) = -\frac{\mu_0 p \sin\varphi}{2\pi r^2} \frac{e(z)\, e(z_0)}{[e'(0)]^2}. \tag{35}$$

From eq. (4) it follows that the leading term of the magnetic field is

$$\mathbf{B}_0^{\text{air}} = \nabla \times \nabla \times (\hat{\mathbf{z}}\chi_e) = -\hat{\mathbf{z}}\nabla_h^2 \chi_e + \nabla_h(\partial_z \chi_e), \tag{36}$$

where ∇_h is the horizontal projection of ∇, or in components

$$B_{0r}^{\text{air}}(\mathbf{r}) = +\frac{\mu_0 p \sin\varphi}{\pi r^3} \frac{e'(z)\, e(z_0)}{[e'(0)]^2}, \tag{37}$$

$$B_{0\varphi}^{\text{air}}(\mathbf{r}) = -\frac{\mu_0 p \cos\varphi}{2\pi r^3} \frac{e'(z)\, e(z_0)}{[e'(0)]^2}, \tag{38}$$

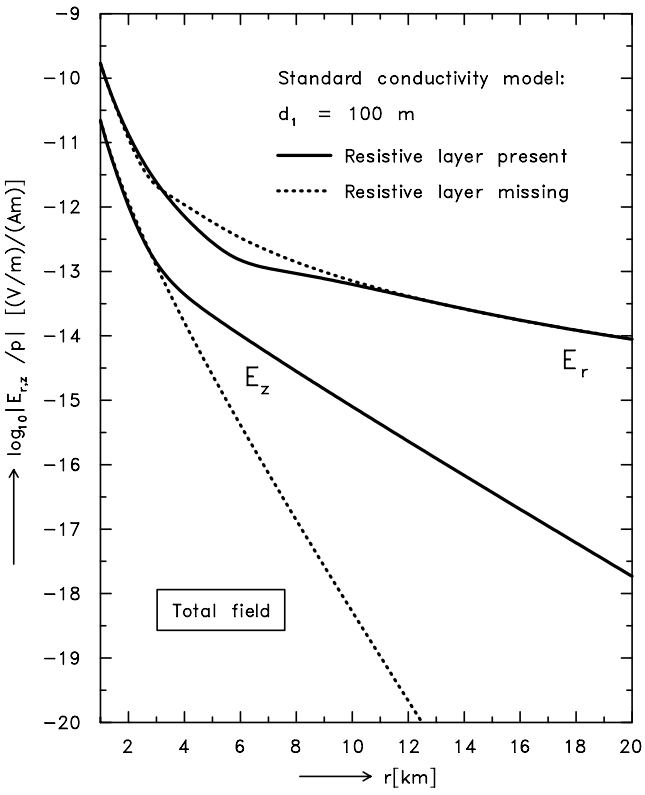

Figure 5. Standard conductivity model of Fig. 1 with $d_1 = 100$ m, $z = z_0 = 100^-$ m (i.e. immediately above sea-bottom) and $f = 0.5$ Hz: shown is E_r and E_z for the standard model (solid lines) and for a modified model, in which the target layer has the conductivity of the background (dotted). Component E_z is not affected by the airwave and, therefore, decays exponentially (straight portions of the two lower graphs).

$$B_{0z}^{\rm air}(\mathbf{r}) = +\frac{3\mu_0\, p \sin\varphi}{2\pi r^4}\,\frac{e(z)\,e(z_0)}{[e'(0)]^2}. \tag{39}$$

3.3 The complete airwave

3.3.1 General formulae

The airwave (22) and (23) with its $1/r^3$-decay is only the leading term in an asymptotic expansion in powers of $1/r$. The asymptotic expansion (28) and Fig. 4 show that contributions of order $1/r^5$ have been neglected. Now a more complete (but less useful) representation of the airwave is considered. Since the TM-mode electric field is confined to the conducting earth and is not linked to the air half-space, the airwave, guided at the air–earth interface, is a TE-mode phenomenon. Therefore, according to eq. (14), the horizontal components are interrelated by

$$E_r^{\rm air}(\mathbf{r}) = (1/r) f(z\,|\,z_0, r)\cos\varphi, \quad E_\varphi^{\rm air}(\mathbf{r}) = -\partial_r f(z\,|\,z_0, r)\sin\varphi. \tag{40}$$

For this reason the discussion is confined to the radial component $E_r^{\rm air}(\mathbf{r})$. If required, $E_\varphi^{\rm air}(\mathbf{r})$ is then obtained via eq. (40). Since the contributions from $Q_m(z|z_0, \kappa)$ and from the even part of $Q_e(z|z_0, \kappa)$ decay for $r \to \infty$ faster than any power of $1/r$, the far-field of E_r is dominated by the odd part of Q_e, which leads to a decay in powers of $1/r$. From eqs (15) and (28) the asymptotic expansion of the complete airwave is

$$E_r^{\rm air}(\mathbf{r}) = -\frac{i\omega\mu_0 p\cos\varphi}{2\pi}\sum_{m=0}^{\infty}\binom{-1/2}{m}\frac{Q_e^{(2m+1)}(z\,|\,z_0, 0)}{r^{2m+3}}. \tag{41}$$

There are different functions, defined in $r > 0$, which lead to this asymptotic expansion. They differ by terms which decay faster than any power of $1/r$ and, therefore, remain invisible in the expansion (41). Defining the odd part of Q_e as

$$Q_e^{\rm odd}(z\,|\,z_0, \kappa) := [Q_e(z\,|\,z_0, \kappa) - Q_e(z\,|\,z_0, -\kappa)]/2, \tag{42}$$

two possible completions of the series (41) in the range $r > 0$ are

$$E_{1r}(\mathbf{r}) := -\frac{i\omega\mu_0 p\cos\varphi}{2\pi r}\int_0^\infty Q_e^{\rm odd}(z\,|\,z_0, \kappa) J_1(\kappa r)\,{\rm d}\kappa \tag{43}$$

and

$$E_{2r}(\mathbf{r}) := -\frac{\omega\mu_0 p\cos\varphi}{\pi^2 r}\int_0^\infty Q_e^{\rm odd}(z\,|\,z_0, it) K_1(tr)\,{\rm d}t, \tag{44}$$

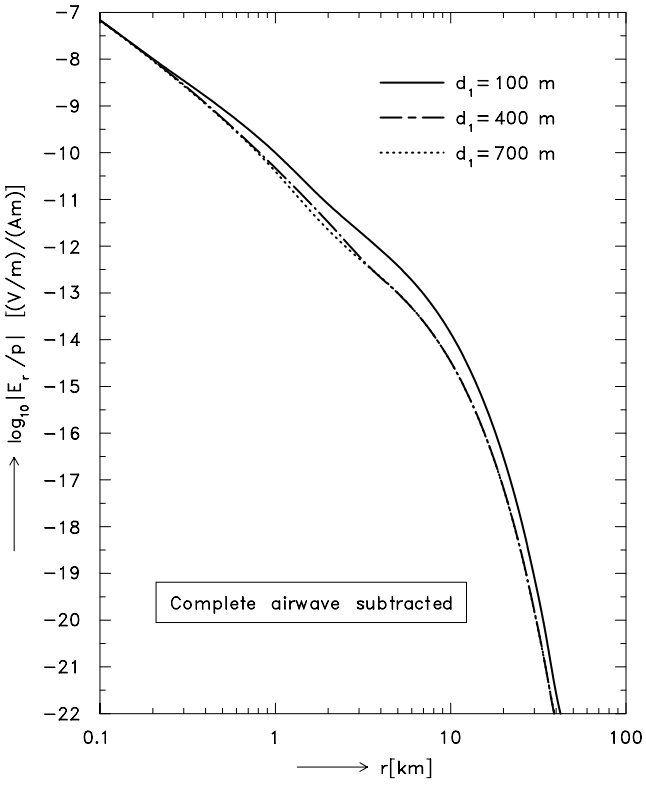

Figure 6. Subtraction of the complete airwave E_{2r} defined in eq. (44). In the far-field, the remainder shows to a high approximation an exponential decay with amplitude and decay length slightly depending on d_1. It represents the resistive-layer mode, discussed in detail in Section 4.3. See also the dotted line in Fig. 13.

where $K_1(\cdot)$ is the modified Bessel function of second kind and order one. The assertion immediately follows from the Taylor expansion

$$Q_e^{\mathrm{odd}}(z \mid z_0, \kappa) = \sum_{m=0}^{\infty} Q_e^{(2m+1)}(z \mid z_0, 0) \frac{\kappa^{2m+1}}{(2m+1)!} \tag{45}$$

and the two integrals (Gradshteyn & Ryzhik 1980, formulae 6.561.14 and 6.561.16)

$$\lim_{\epsilon \to 0^+} \int_0^{\infty} \frac{\mathrm{e}^{-\epsilon\kappa} \kappa^{2m+1}}{(2m+1)!} J_1(\kappa r)\, \mathrm{d}\kappa = \frac{2}{i\pi} \int_0^{\infty} \frac{(it)^{2m+1}}{(2m+1)!} K_1(tr)\, \mathrm{d}t = \binom{-1/2}{m} \frac{1}{r^{2m+2}}. \tag{46}$$

The justification of eq. (44), based on properties of $Q_e(z|z_0, \kappa)$ in the complex κ-domain, is postponed to Section 4.2. For $r \to 0$, completion E_{1r} is $\mathcal{O}(1)$ and E_{2r} is $\mathcal{O}(1/r^2)$. Although eq. (43) is the more obvious completion, eq. (44) will turn out to be the more natural one.

If the airwave is strictly understood as the wave guided at the air–ocean interface, then only the unique asymptotic expansion (41) in powers of $1/r$ is available. In a wider sense, however, the airwave is sometimes defined as the difference between the observed electromagnetic signal for finite water depth d_1 and the signal for infinite water depth, $d_1 = \infty$,

$$E_{3r}(\mathbf{r}) := E_r(\mathbf{r}, d_1) - E_r(\mathbf{r}, \infty). \tag{47}$$

The airwave in this definition also includes the reflections at the air–ocean interface, which show an exponential decay with separation r. Moreover, E_{3r} contains contributions from the TM-mode and, therefore, is no longer a pure TE-mode. Completion $E_{2r}(\mathbf{r})$, in which all reflections are filtered out, is the purest airwave, the mixed completion $E_{1r}(\mathbf{r})$ takes in addition some reflections into account, and all reflections are considered in $E_{3r}(\mathbf{r})$. The three significantly different definitions of the airwave show an identical far-field behaviour. However, it also turns out that in the intermediate r-range they differ only slightly.

Fig. 6 shows the data of Fig. 3 after subtracting the complete airwave (44). The remainder is essentially an exponentially decaying wave representing the response from the resistive layer.

3.3.2 Example: uniform half-space

As the simplest example consider a uniform half-space of conductivity σ. With $k^2 := i\omega\mu_0\sigma$ and $\alpha^2 := \kappa^2 + k^2$, the kernel Q_e and its decomposition into even and odd part gives

$$Q_e(z \mid z_0, \kappa) = \frac{1}{2\alpha} \left[\mathrm{e}^{-\alpha|z-z_0|} + \frac{\alpha - \kappa}{\alpha + \kappa} \mathrm{e}^{-\alpha(z+z_0)} \right], \tag{48}$$

$$Q_e^{\rm even}(z\,|\,z_0,\kappa)=\frac{1}{2\alpha}\left[{\rm e}^{-\alpha|z-z_0|}+\frac{\alpha^2+\kappa^2}{k^2}{\rm e}^{-\alpha(z+z_0)}\right], \tag{49}$$

$$Q_e^{\rm odd}(z\,|\,z_0,\kappa)=-\frac{\kappa}{k^2}{\rm e}^{-\alpha(z+z_0)}. \tag{50}$$

The two alternative representations of the airwave derived from eqs (43) and (44) are

$$E_{1r}(\mathbf{r})=\frac{p\cos\varphi}{2\pi\sigma r}\int_0^\infty \kappa\,{\rm e}^{-\alpha(z+z_0)}J_1(\kappa r)\,{\rm d}\kappa \tag{51}$$

and

$$E_{2r}(\mathbf{r})=\frac{p\cos\varphi}{\pi^2\sigma r}\int_0^\infty t\,{\rm e}^{-\beta(z+z_0)}K_1(tr)\,{\rm d}t,\quad \beta^2:=k^2-t^2, \tag{52}$$

or in closed form (Gradshteyn & Ryzhik 1980, formulae 6.637.1 and 6.637.3)

$$E_{1r}(\mathbf{r})=\frac{p\cos\varphi}{2\pi\sigma r}\,\partial_{rz}^2[I_0(w_-)K_0(w_+)] \tag{53}$$

and

$$E_{2r}(\mathbf{r})=\frac{p\cos\varphi}{2\pi^2 i\sigma r}\,\partial_{rz}^2\big[K_0({\rm e}^{-\pi i}w_-)K_0(w_+)\big], \tag{54}$$

where $I_0(\cdot)$ and $K_0(\cdot)$ are modified zero-order Bessel functions of the first and second kind and

$$w_\pm:=(k/2)[R_+\pm(z+z_0)]\ \text{ with }\ R_+^2:=r^2+(z+z_0)^2. \tag{55}$$

The notation ${\rm e}^{-\pi i}w_-$ ensures the correct selection of the Riemannian sheet of $K_0(w)$, which has a (logarithmic) branch cut along the negative real axis. Since $\arg(w_-)=\pi/4$, the phase of ${\rm e}^{-\pi i}w_-$ is $-3\pi/4$, which lies in the same sheet as w_-, whereas ${\rm e}^{+\pi i}w_-$ would lie in a different sheet.

From the identity

$$\pi i\,I_0(w)=K_0({\rm e}^{-\pi i}w)-K_0(w) \tag{56}$$

(Abramowitz & Stegun 1972, formula 9.6.31) it follows that

$$E_{1r}(\mathbf{r})-E_{2r}(\mathbf{r})=-\frac{p\cos\varphi}{2\pi^2 i\sigma r}\,\partial_{rz}^2[K_0(w_-)K_0(w_+)]. \tag{57}$$

Explicit expressions of eqs (53), (54) and (57) are given in Appendix B1.

The leading terms of the asymptotic expansions of the modified Bessel functions (Abramowitz & Stegun 1972, formulae 9.7.1 and 9.7.2)

$$I_0(w)={\rm e}^w/\sqrt{2\pi w}\,[1+\mathcal{O}(1/w)],\quad K_0(w)={\rm e}^{-w}\sqrt{\pi/(2w)}\,[1+\mathcal{O}(1/w)] \tag{58}$$

reveal that

$$I_0(w_-)K_0(w_+)\approx K_0\big({\rm e}^{-\pi i}w_-\big)K_0(w_+)/(\pi i)\approx {\rm e}^{-k(z+z_0)}/(kr), \tag{59}$$

$$K_0(w_-)K_0(w_+)/(\pi i)\approx {\rm e}^{-kR_+}/(ikr). \tag{60}$$

From eq. (60) the difference (57) between the two completions $E_{1r}(\mathbf{r})$ and $E_{2r}(\mathbf{r})$ becomes exponentially small for $r\to\infty$. Moreover, eq. (59) in conjunction with eqs (53) and (54) shows that in this limit both completions tend to the leading term (25) of the airwave. The subsequent terms, derived with eq. (50) from eq. (41), give

$$E_r^{\rm air}(\mathbf{r})=\frac{p\,{\rm e}^{-k(z+z_0)}\cos\varphi}{2\pi\sigma r^3}\left[1+\frac{3\zeta}{2\varrho^2}+\frac{45\zeta(1+\zeta)}{8\varrho^4}+\mathcal{O}\left(\frac{1}{\varrho^6}\right)\right], \tag{61}$$

where $\varrho:=kr$ and $\zeta:=k(z+z_0)$. For the uniform half-space, the different definitions E_{1r}, E_{2r} and E_{3r} of the complete airwave are compared in Fig. 7. Since it turns out that the three completions give very similar results, for clarity only differences are shown.

The even parts of the integral kernels produce contributions with a fast exponential r-decay: The TM-mode kernel

$$Q_m(z\,|\,z_0,\kappa)=\frac{\alpha}{2k^2}\left[{\rm e}^{-\alpha|z-z_0|}+{\rm e}^{-\alpha(z+z_0)}\right] \tag{62}$$

and the even part eq. (49) of $Q_e(z|z_0,\kappa)$ give rise to contributions with dominating terms ${\rm e}^{-kR_-}$ and ${\rm e}^{-kR_+}$, where $R_\pm^2:=r^2+(z\pm z_0)^2$. The two exponentials describe, respectively, the direct wave and the wave reflected at $z=0$.

4 GUIDED WAVES IN THE COMPLEX WAVENUMBER PLANE

4.1 Analytical properties of the integral kernels

The guided waves considered in this study are best described by generalizing the real wavenumber κ to complex values and investigating the singularities of the integral kernels in the complex wavenumber domain. Then the airwave can be identified with a branch cut integral along the positive imaginary axis and the resistive-layer mode, introduced in Section 1, is the contribution from a pole close to the origin $\kappa=0$.

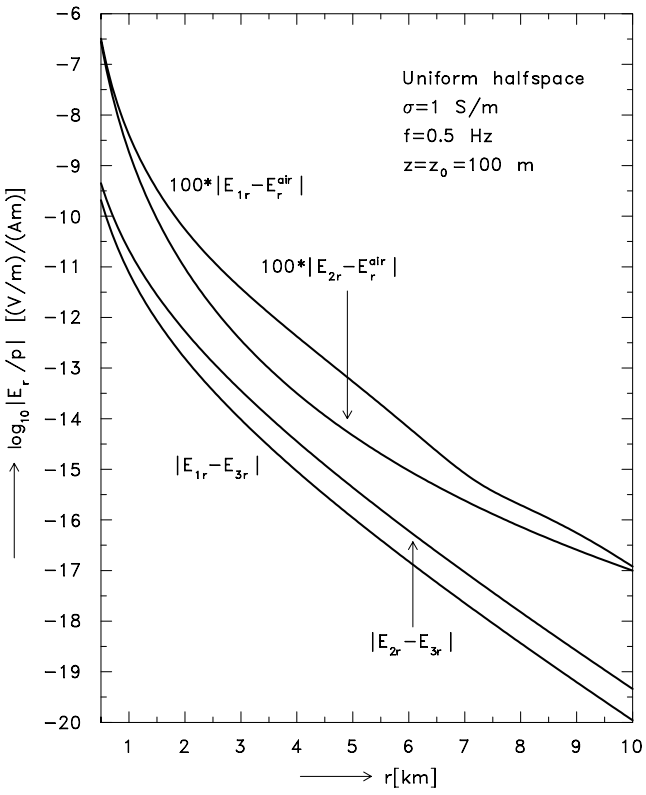

Figure 7. Complete airwave: comparison of different completions for a uniform half-space. The airwaves E_{1r}, E_{2r} and E_{3r}, defined, respectively, in eqs (43), (44) and (47), have an identical far-field behaviour, but are influenced differently by shortranging reflections at the air–ocean interface. E_{3r}, the difference of E_r to an ocean of infinite depth, contains all reflections, the 'mixed' airwave E_{1r} is only partly influenced by reflections, and the 'pure' airwave E_{2r} is not influenced at all. This is illustrated by the two lower graphs showing that E_{3r} is closer to E_{1r} than to E_{2r}. The two upper graphs, raised for clarity by two decades, illustrate that E_r^{air}, represented in eq. (61) by the first three asymptotic terms, is closer to the pure airwave E_{2r} than to E_{1r} with its contributions from surface reflections. In fact, $|E_{2r} - E_r^{\text{air}}|$ equals almost exactly the first neglected term $\sim 1/r^9$ of eq. (61).

Conventionally, the electric field components in marine CSEM are presented in terms of Hankel transforms as in eqs (15) and (16). This is a superposition of oscillating fields with real wavenumber κ, where the decay for $r \to \infty$ is achieved by destructive interference. For the airwave considered so far, this presentation was sufficient. However, for a deeper understanding and in particular for the wave guided in a resistive layer, an extension of the real wavenumber description to complex wavenumbers is useful. The fundamentals of this description, mostly restricted to TE-mode sources (vertical magnetic dipoles), are given by Kaufman & Keller (1983, pp. 432–445) and Goldman (1990, chapter 2). In the complex κ-plane, the r-dependence of the fields is presented by a superposition of damped oscillations, originating from the singularities (poles and branch cuts) of the integral kernels $Q_e(z|z_0, \kappa)$ and $Q_m(z|z_0, \kappa)$. This warrants a closer look into the analytical properties of these kernels.

For real wavenumbers κ, the kernel $Q_e(z|z_0, \kappa)$ has an even and odd part. The odd part comes from integrating the Riccati equation (A8) with the initial value $a_e(0, \kappa) = \kappa \geq 0$. In the extension to complex wavenumbers, this assignment is changed: We assume an air half-space with a small conductivity σ_0 and define $k_0^2 := i\omega\mu_0\sigma_0$, $\alpha_0^2 := \kappa^2 + k_0^2$. Then $f_{ea}(z) \sim \exp(\alpha_0 z)$, $z \leq 0$, yields in the limit $\sigma_0 \to 0$

$$a_e(0, \kappa) = \lim_{\sigma_0 \to 0} \alpha_0 = \sqrt{\kappa^2} = \begin{cases} +\kappa & \text{for} \quad \text{Re}(\kappa) > 0, \\ -\kappa & \text{for} \quad \text{Re}(\kappa) < 0. \end{cases} \tag{63}$$

This new definition of the initial value satisfies the symmetry $a_e(0, -\kappa) = a_e(0, \kappa)$. Therefore, the integration of eq. (A8) gives a transfer function $a_e(z, \kappa)$, which is symmetric in κ. As a consequence, $Q_e(z|z_0, \kappa)$ now is a symmetric function in the complex plane. Mathematically this has become possible by introducing via eq. (63) two branch cuts along the positive and negative imaginary axes, where the imaginary part of $\sqrt{\kappa^2}$ is discontinuous. These branch cuts of α_0 lead from $\kappa = +ik_0$ to $\kappa = +i\infty$ and from $\kappa = -ik_0$ to $\kappa = -i\infty$.

Due to the point-symmetry $Q_{e,m}(z|z_0, -\kappa) = Q_{e,m}(z|z_0, \kappa)$, a singularity in the upper κ-halfplane has its correspondence in the lower halfplane. Without loss of generality we, therefore, confine our attention to the upper κ-halfplane. The basic integral representations (15) and (16) involve both $J_1(x)$ and $J_1'(x)$. For the asymptotic approach in Section 3.1, the asymptotic expansion of $J_1'(x)$ was accessible by differentiating the simple asymptotic series (28). For general argument x, the exact formula $J_1'(x) = J_0(x) - J_1(x)/x$ is used. Therefore, $J_0(x)$ is now also included and eq. (26) is extended to

$$g_n(r) := \int_0^\infty f(\kappa)\, J_n(\kappa r)\, \mathrm{d}r, \quad n = 0, 1. \tag{64}$$

By general relations (Abramowitz & Stegun 1972, formulae 9.1.3, 9.1.4 and 9.1.39) the Bessel functions $J_n(\cdot)$ in eq. (64) are replaced by the Hankel functions $H_n^{(1)}(\cdot)$ of the first kind,

$$J_n(z) = \frac{1}{2}\left[H_n^{(1)}(z) - \mathrm{e}^{n\pi i} H_n^{(1)}(z\mathrm{e}^{\pi i})\right]. \tag{65}$$

$H_n^{(1)}(z)$ is an analytic function of z throughout the z-plane cut along the negative axis and shows for $|z| \to \infty$ the asymptotic behaviour (Abramowitz & Stegun 1972, formula 9.2.3)

$$H_n^{(1)}(z) \approx \sqrt{2/(\pi z)}\,\exp\left[+i(z - n\pi/2 - \pi/4)\right], \quad -\pi < \arg z < 2\pi. \tag{66}$$

In particular, $H_n^{(1)}(z)$ vanishes for $z \to \infty$ in the upper z-halfplane. The argument $z\mathrm{e}^{\pi i}$ in the last term of eq. (65) implies that for $z > 0$ a point immediately *above* the cut along the negative axis is taken. The occurrence of $H_n^{(1)}(\cdot)$ rather than $H_n^{(2)}(\cdot)$ reflects the decision to use the upper κ-halfplane.

Now the one-sided infinite Bessel function integrals $g_n(r)$ in eq. (64) are transformed with eq. (65) into a two-sided infinite integral, using for $\kappa < 0$ the change of variable $\kappa \to -\kappa$,

$$g_0(r) = \frac{1}{2}\int_{-\infty}^{\infty} f(\kappa)\, H_0^{(1)}(\kappa r)\,\mathrm{d}\kappa, \tag{67}$$

where $f(\kappa)$ has been completed by $f(-\kappa) = -f(\kappa)$. Since $H_1^{(1)}(z) \approx 2/(i\pi\, z)$ for $z \to 0$, the pole at $\kappa = 0$ requires a slight modification,

$$g_1(r) = \frac{1}{2}⨍_{-\infty}^{+\infty} f(\kappa)\, H_1^{(1)}(\kappa r)\,\mathrm{d}\kappa = \frac{f(0)}{r} + \frac{1}{2}\int_{-\infty}^{+\infty} f(\kappa)\, H_1^{(1)}(\kappa r)\,\mathrm{d}\kappa. \tag{68}$$

In the first integral, the Cauchy principal value is taken and the second integral requires a small indentation of the contour above the pole. Used was the even completion $f(-\kappa) = f(\kappa)$.

The analyticity of $H_n^{(1)}(\kappa\, r)$ in the upper κ-plane with its exponential decay at infinity and the 'good behaviour' of the integral kernels for $|\kappa| \to \infty$ (see for instance, eqs 48 and 62) will allow the (indented) real-axis contour to deform into a contour around selected singularities of $f(\kappa)$, which will be identified with the guided waves.

The construction of the transfer functions $a_{e,m}(z, \kappa)$ and $b_{e,m}(z, \kappa)$ in Appendix A2 via the integration of the corresponding Riccati equations shows that these transfer functions inherit their branch cuts from the initial values. Recalling that σ_t is the uniform terminating conductivity at (great) depth, $b_e(z, \kappa)$ and $b_m(z, \kappa)$ have a branch cut from $\kappa = +ik_t$ to $\kappa = +i\infty$, $k_t^2 := i\omega\mu_0\sigma_t$, inherited from $b_e(z_t, \kappa) = \alpha_t(\kappa)$ and $b_m(z_t, \kappa) = \alpha_t(\kappa)/\sigma_t$. The branch cut of $a_e(z, \kappa)$ along the positive imaginary axis results from eq. (63), whereas $a_m(z, \kappa)$ is free of branch cuts; it is a meromorphic function. With these results it is seen, via eq. (Am) from eqs (17) and (18), that the branch lines of $Q_e(z|z_0, \kappa)$ are those of $\alpha_0(\kappa)$ and $\alpha_t(\kappa)$, whereas only the branch line of the latter is present in $Q_m(z|z_0, \kappa)$.

Now we turn to the poles of the integral kernels. The position of the poles is an intrinsic feature of conductivity structure and frequency, independent of the position of source and/or receiver. Let

$$D_e(z, \kappa) := a_e(z, \kappa) + b_e(z, \kappa) \quad \text{and} \tag{69}$$

$$D_m(z, \kappa) := a_m(z, \kappa) + b_m(z, \kappa) \tag{70}$$

be the denominators of the integral kernels (17) and (18). Suppressing the subscripts e, m specifying the mode for ease of notation, and recalling the definitions (20) and (21), the Wronskian

$$f_a(z, \kappa) f_b(z, \kappa) D(z, \kappa) = W(z, \kappa) =: \overline{D}(\kappa) \tag{71}$$

is independent of z and the pole positions are the zeroes of $\overline{D}(\kappa)$. Let $\overline{D}(\kappa_0) = 0$. Because of $W(z, \kappa_0) = 0$, the linear independence of f_a and f_b breaks down at $\kappa = \kappa_0$ and $f_a(z, \kappa_0)$ becomes a multiple of $f_b(z, \kappa_0)$, that is, $f_a(z, \kappa_0) = \gamma\, f_b(z, \kappa_0)$, $\gamma \neq 0$. Since these functions are specified only up to a constant factor, $\gamma = 1$ can be taken without loss of generality. Therefore,

$$f_a(z, \kappa_0) = f_b(z, \kappa_0) =: f_0(z). \tag{72}$$

The function $f_0(z)$, defined for the TE-mode in the range $-\infty < z < +\infty$ and for the TM-mode in the range $0 < z < \infty$, vanishes at both ends of the interval and is a square-integrable eigensolution of eq. (10) (TE-mode) or eq. (12) (TM-mode). The eigenvalue is $\kappa = \kappa_0$. The quantities κ_0 and $f_0(z)$ define a bound state or discrete mode. The properties of these modes are described in detail by Chew (1995, chapter 6). A particular bound state, namely the resistive layer mode, is the focus of Section 4.3.

Since $f_0(z)$ does not vanish identically in z, a value of z with $f_0(z) \neq 0$ can be found. Then a zero $\kappa = \kappa_0$ of $\overline{D}(\kappa)$ is also a zero of $D(z, \kappa)$. The region of possible zeroes of $D(z, \kappa)$ in the κ-plane is identified in the following way. After multiplying the differential eqs (10) and (12) by their complex conjugate solutions, integrating by parts, and using the definitions (11) and (13), the integral representations are, recalling the definition of α^2 in (10) and retaining only the most important arguments,

$$a_e(z) = \int_{-\infty}^{z} \left[|f_{ea}'|^2 + \alpha^2 |f_{ea}|^2\right] \mathrm{d}t / |f_{ea}(z)|^2, \tag{73}$$

$$b_e(z) = \int_{z}^{\infty} \left[|f_{eb}'|^2 + \alpha^2 |f_{eb}|^2\right] \mathrm{d}t / |f_{eb}(z)|^2, \tag{74}$$

$$a_m(z) = \int_{0^+}^{z} (1/\sigma)[|f'_{ma}|^2 + \alpha^2 |f_{ma}|^2]\, \mathrm{d}t/|f_{ma}(z)|^2, \tag{75}$$

$$b_m(z) = \int_{z}^{\infty} (1/\sigma)[|f'_{mb}|^2 + \alpha^2 |f_{mb}|^2]\, \mathrm{d}t/|f_{mb}(z)|^2. \tag{76}$$

Let the conductivity in $z > 0$ be bounded by

$$0 < \sigma_{\min} \le \sigma(z) \le \sigma_{\max} < \infty. \tag{77}$$

With $\kappa =: u + iv$ it follows from eqs (69) and (70), using eqs (73)–(77) and

$$\alpha^2(z, \kappa) = u^2 - v^2 + i[2uv + \omega\mu_0\sigma(z)], \tag{78}$$

that

$$\begin{aligned} \mathrm{Re}(D_{e,m}) &> 0 \quad \text{for} \quad \mathrm{Re}(\kappa^2) = u^2 - v^2 \ge 0, \\ \mathrm{Im}(D_{e,m}) &< 0 \quad \text{for} \quad \mathrm{Im}(\kappa^2) = 2uv \le -\omega\mu_0\sigma_{\max}, \\ \mathrm{Im}(D_m) &> 0 \quad \text{for} \quad \mathrm{Im}(\kappa^2) = 2uv \ge -\omega\mu_0\sigma_{\min}, \\ \mathrm{Im}(D_e) &> 0 \quad \text{for} \quad \mathrm{Im}(\kappa^2) = 2uv \ge 0. \end{aligned} \tag{79}$$

The conditions (79) define regions in the κ-plane, where the real or imaginary part of the denominators $D_{e,m}$ has a definite sign. The zeroes of $D_{e,m}(z, \kappa)$, corresponding to the zeroes of $\overline{D}_{e,m}(\kappa)$, lie in the complementary part of the plane.

Next, the pole condition $\overline{D}(\kappa) = 0$ is formulated in terms of conditions on the zeroes of transfer functions at $z = 0$, where these conditions attain the simplest form. Applying eq. (71) at $z = 0$ with $f'_{ea}(0, \kappa) = \sqrt{\kappa^2}\, f_{ea}(0, \kappa)$ and $f_{ma}(0, \kappa) = 0$ for all κ, but $f_{mb}(0, \kappa) = 0$ only for $\kappa = \kappa_0$ (see eq. 72), with the definitions (11), (13), (20) and (21), the result is

$$\sqrt{\kappa^2} + b_e(0, \kappa) = 0, \qquad 1/b_m(0, \kappa) = 0, \tag{80}$$

where the square root $\sqrt{\kappa^2}$ is interpreted as in eq. (63). The disadvantage of formulating the pole conditions at $z = 0$ is that the pole position associated with a deep structure (as the resistive-layer pole discussed in Section 4.3) is extremely sharp and might escape detection when scanning the κ-plane. Therefore, use of the local condition $D(z, \kappa) = 0$, with a value of z in the depth range of interest, will be preferable.

Fig. 8 diagrams the analytical properties of Q_e and Q_m in the upper κ-halfplane. (With point symmetry at $\kappa = 0$, the same singularities occur in the lower halfplane.) Also shown are the branch cuts of $H_n^{(1)}$ and the pole $\kappa = 0$ of $H_1^{(1)}$ (see eq. 68). Therefore, the origin $\kappa = 0$ is a very exceptional point. It is a branch point both of Q_e and the Hankel functions and in addition it is a pole of $H_1^{(1)}$. For conceptional simplicity, the situation near $\kappa = 0$ is disentangled by assigning a small positive conductivity σ_0 to the air, which separates the corresponding branch points ik_0 and 0. The result is the clarified picture shown in Fig. 8. After this explanation, however, all further discussions will be restricted again to the limit $\sigma_0 \to 0^+$. This is justified, since the pole $\kappa = 0$ does not contribute to E_r and E_φ: The residual, which according to (15) and (16) is $\sim [Q_e(\kappa = 0) - Q_m(\kappa = 0)]/r^2$, vanishes in view of (29).

All singularities of Q_e and Q_m lie in the 'triangular' region bounded by $\mathrm{Im}(\kappa^2) = -\omega\mu_0\sigma_{\max}$, $\mathrm{Re}(\kappa^2) = 0$ and $\mathrm{Im}(\kappa^2) = 0$. Two branch cuts occur: the first from $\kappa = 0$ to $\kappa = i\infty$ associated with the air–half-space and the second from $\kappa = ik_t$ to $\kappa = i\infty$ associated with the terminating uniform half-space. There is some freedom in the selection of the branch line connecting the branch points. We have chosen the branch line along which $\mathrm{Re}(\sqrt{\kappa^2}) = 0$ and $\mathrm{Re}(\alpha_t) = 0$, where the latter condition is equivalent to $\mathrm{Im}(\kappa^2) = -\omega\mu_0\sigma_t$. Then $\mathrm{Re}(\sqrt{\kappa^2}) > 0$ and $\mathrm{Re}(\alpha_t) > 0$ outside the branch lines. When crossing the respective branch lines, $\mathrm{Im}(\sqrt{\kappa^2})$ and $\mathrm{Im}(\alpha_t)$ change sign, with positive values attained at the right bank.

The existence and position of poles depend on the conductivity layering, with the most general situation shown in Fig. 8. For instance, in the degenerate case of a uniform half-space all poles are missing and only the two branch cuts occur. The difference in the nature of TE- and TM-mode (inductive and galvanic coupling) introduces differences in the distribution of poles associated with these modes. For the TM-mode a thin resistive layer is a barrier, whereas the TE-mode easily bridges it. As a consequence, TM-mode energy can be trapped between two resistive layers or between the air–ocean interface and a resistive layer at depth, with the consequence that the energy bounces between the barriers. This gives rise to an infinite series of TM-mode poles, which can be investigated by means of the 'standard model'.

The position of poles for this model is shown in Fig. 9. There is only one TE-mode pole, but an infinite number of TM-mode poles, from which only the first seven are shown. Distinctly separated from the six other poles is the pole associated with the resistive layer of conductivity $\sigma_r = 0.01\ \mathrm{S\,m^{-1}}$ between $z = 2000$ and 2100 m (see Fig. 1). This pole is discussed in detail in Section 4.3. The other TM-mode poles, which form a regular pattern with three pairs of two poles, describe a system of highly damped trapped modes between the air–ocean interface at $z = 0$ and the resistive layer at $z = 2000$ m. Let the sea have the depth d_1 and the conductivity σ_1 and assign to the ocean sediments between ocean bottom and resistive layer the thickness d_2 and the conductivity σ_2. For the 'standard model' with $d_1 = d_2$ and the total thickness $D := d_1 + d_2$ of the conducting layers, simple approximate expressions exist for the position of the TM-mode poles in the regular pole pattern. Ordering the poles κ_n in ascending order of $\mathrm{Im}\,(\kappa_n)$, we find for pair m, asymptotically valid for $m \gg 1$ (see Appendix B2),

$$\kappa_n^2 \approx \begin{cases} -\dfrac{n^2\pi^2}{D^2} - i\omega\mu_0 \dfrac{2\sigma_1\sigma_2}{\sigma_1 + \sigma_2}, & n = 2m - 1, \\ -\dfrac{n^2\pi^2}{D^2} - i\omega\mu_0 \dfrac{\sigma_1^2 + \sigma_2^2}{\sigma_1 + \sigma_2}, & n = 2m. \end{cases} \tag{81}$$

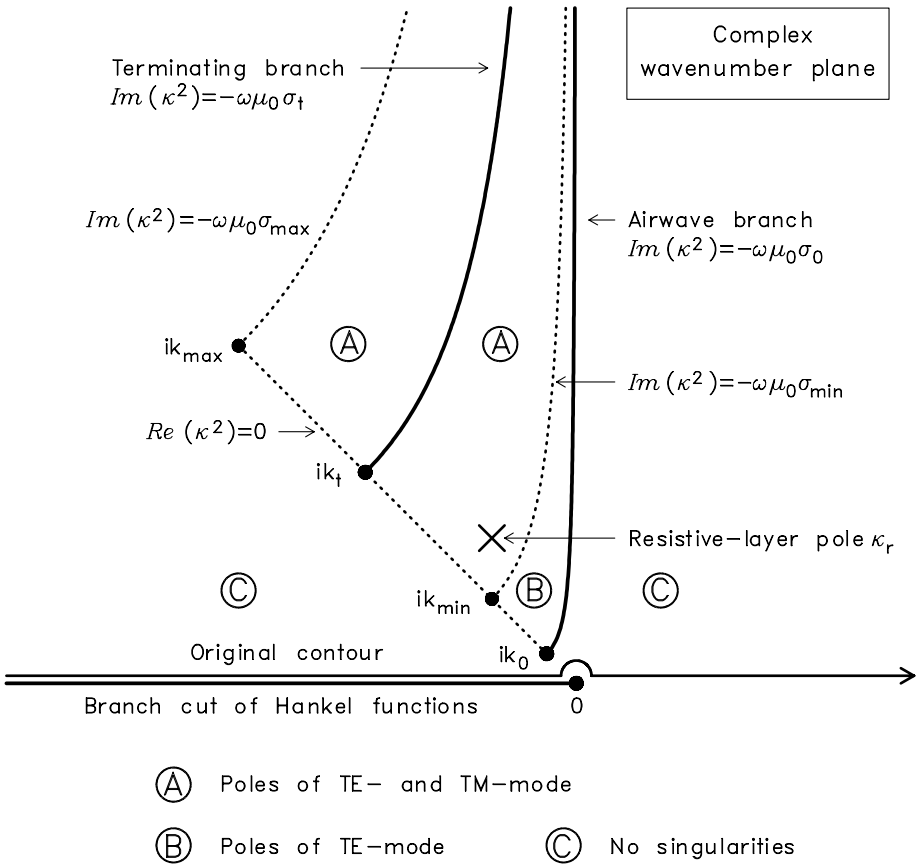

Figure 8. Schematic view of the analytical properties of the Bessel function integral kernel and the Hankel functions $H_n^{(1)}(\kappa r)$ in the complex κ-domain. Shown are the relevant lines $\mathrm{Im}(\kappa^2) = -\omega\mu_0\sigma$, where σ is either one of the bounds $\sigma_{\max}$ or $\sigma_{\min}$ defined in eq. (77) or the conductivity σ_t or σ_0 of one of the bounding half-spaces (terminating half-space or air half-space). Branch cuts (solid lines) are associated only with the latter. The finite endpoints are given by $\kappa = ik = (-1+i)\sqrt{\omega\mu_0\sigma/2}$. Marked is also the pole $\kappa = 0$ of $H_1^{(1)}(\kappa r)$. For conceptual clarity, a small positive conductivity σ_0 is assigned to the air half-space. This assumption, however, is dropped in the sequel. The singularities with the smallest imaginary part determine the far-field behaviour: the branch $\mathrm{Im}(\kappa^2) = -\omega\mu_0\sigma_0 = 0$ yields the pure airwave and the pole κ_r close to $ik_{\min}$ gives the resistive-layer mode. Shown is the most general situation: in specific models some regions are void of poles and a distinct resistive-layer pole does not exist.

For a uniformly conducting slab with $\sigma_1 = \sigma_2 := \sigma$, the poles are asymptotically aligned along $\mathrm{Im}(\kappa^2) = -\omega\mu_0\sigma$ and are given by

$$\kappa_n^2 \approx -(n\pi/D)^2 - i\omega\mu_0\sigma. \tag{82}$$

This formula becomes exact for $\sigma_r \to 0$, see eq. (B10). A comparison of exact and approximate positions of the first six trapped TM-mode poles gives Table 1.

The TE-mode pole of the 'standard model' represents the combined TE-mode effect of the first and second layer. Together with the branch lines $\mathrm{Re}(\sqrt{\kappa^2}) = 0$ (associated with the air half-space) and $\mathrm{Re}(\alpha_t) = 0$ (associated with the terminating layer), all important TE-mode constituents are represented by singularities of Q_e, whereas the resistive layer with its marginal influence onto the TE-mode, remains invisible.

Table 1. Comparison of exact TM-mode pole positions from Fig. 9 with the approximations obtained from eq. (81) with $\sigma_1 = 3\ \mathrm{S\,m^{-1}}$, $\sigma_2 = 1\ \mathrm{S\,m^{-1}}$, $D = 2000$ m and $\omega = 3.142\ \mathrm{s^{-1}}$.

	$1000 \times \kappa_n\ (\mathrm{m^{-1}})$	
n	Exact	Approximate
1	$-1.193 + i2.209$	$-1.405 + i2.107$
2	$-1.544 + i3.407$	$-1.430 + i3.452$
3	$-0.601 + i4.781$	$-0.623 + i4.753$
4	$-0.789 + i6.318$	$-0.780 + i6.331$
5	$-0.371 + i7.874$	$-0.377 + i7.863$
6	$-0.525 + i9.436$	$-0.523 + i9.439$

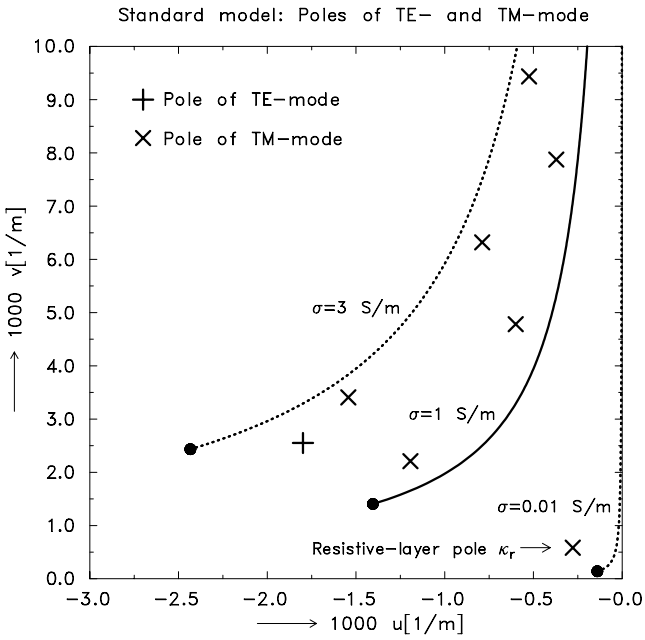

Figure 9. Standard conductivity model of Fig. 1: Position of the poles in the complex plane $\kappa = u + iv$. The frequency is $f = 0.5$ Hz. There is only one TE-mode pole, but an infinite number of TM-mode poles. From these poles are shown the resistive-layer pole and six regular poles from the sequence eq. (81). The solid and dotted lines are the isolines $\mathrm{Im}(\kappa^2) = -\omega\mu_0\sigma$ with σ marked at the graph. In particular, the solid line is the terminating branch. Note the different scales in u- and v-direction.

On the basis of numerical experiments we conjecture that the number of TE-mode poles is always smaller than the number of layers. Region B in Fig. 8 is void of poles, if $\sigma_{\min}$ is small, as in the resistive-layer case. On the other hand, a pole can exist in region B for a model consisting of the air half-space and two layers with the upper layer less conducting than the terminating half-space.

Since $H_n^{(1)}(\kappa r)$ is analytic in the upper κ-halfplane and vanishes according to eq. (66) $\sim \exp(-vr)$ for $v = \mathrm{Im}(\kappa) \to +\infty$, the original contour confined to the real axis (with an indentation above $\kappa = 0$, see Fig. 8), can be deformed to the contour surrounding the triangular region of singularities as shown in Fig. 10. This contour, which does not require knowledge of the poles, can be used to obtain highly precise far-field responses. This is shown by Goldman (1990) for the vertical magnetic dipole. When the position of poles is known, the contour can be contracted around each pole and the response is represented as the sum of the residua at these poles plus the integrals along the two branch cuts. The far-field is then dominated by the poles and branch points with the smallest imaginary part, because these lead to the slowest exponential decay. A pole or branch point at κ_0 is associated with the decay length

$$L_0 = 1/\mathrm{Im}(\kappa_0). \tag{83}$$

4.2 The airwave in the wavenumber plane

In case of the branch cut $\mathrm{Im}(\kappa^2) = 0$, which has a branch point at $\kappa = 0$, the exponential decay has to be replaced by an algebraic decay in terms of powers of $1/r$. The contribution of this branch cut to $E_r(\mathbf{r})$ is obtained by integrating in Fig. 10 along both banks of the branch cut, down along the left bank with $\sqrt{\kappa^2} = -it$ and up along the right bank with $\sqrt{\kappa^2} = +it$ (see eq. 63). Then eqs (15) and (68) yield

$$\begin{aligned}
&-\frac{i\omega\mu_0 p\cos\varphi}{2\pi r}\,\frac{1}{2}\int_{\bigcup} Q_e(z\,|\,z_0,\sqrt{\kappa^2})H_1^{(1)}(\kappa r)\,\mathrm{d}\kappa \\
&= \frac{\omega\mu_0 p\cos\varphi}{2\pi r}\,\frac{1}{2}\int_0^\infty [Q_e(z\,|\,z_0,it) - Q_e(z\,|\,z_0,-it)]H_1^{(1)}(itr)\,\mathrm{d}t \\
&= \frac{\omega\mu_0 p\cos\varphi}{2\pi r}\int_0^\infty Q_e^{\mathrm{odd}}(z\,|\,z_0,it)H_1^{(1)}(itr)\,\mathrm{d}t \\
&= -\frac{\omega\mu_0 p\cos\varphi}{\pi^2 r}\int_0^\infty Q_e^{\mathrm{odd}}(z\,|\,z_0,it)K_1(tr)\,\mathrm{d}t = E_{2r}(\mathbf{r}),
\end{aligned} \tag{84}$$

with Q_e^{odd} and E_{2r} already defined in eqs (42) and (44). Moreover, it has been used that $H_1^{(1)}(itr) = -(2/\pi)K_1(tr)$ (Abramowitz & Stegun 1972, formula 9.6.4). In Section 3.3.1 it was shown that $E_{2r}(\mathbf{r})$ has the asymptotic behaviour (41) of the airwave and, therefore, is a possible completion of the asymptotic series in the range $r > 0$. For this reason the branch $\mathrm{Im}\,(\kappa^2) = -\omega\mu_0\sigma_0 = 0$ in Fig. 8 is called the 'airwave branch'.

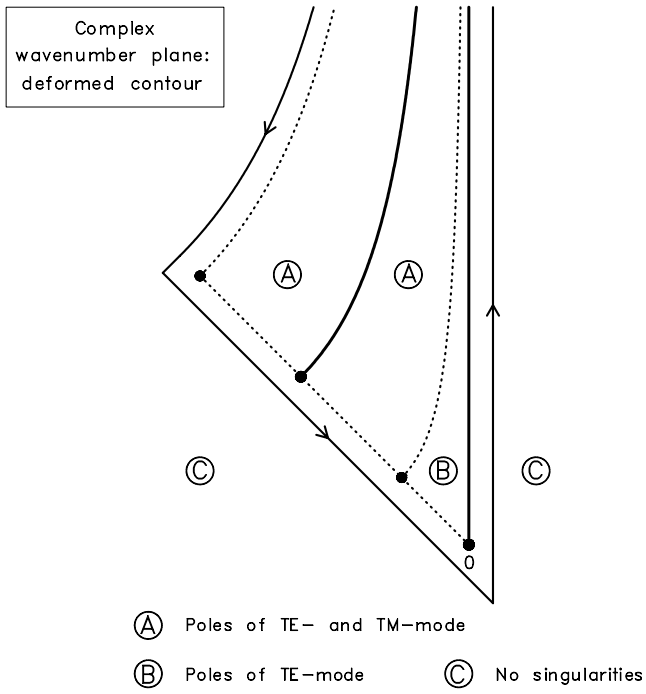

Figure 10. Deformation of the contour, originally confined to the real axis (see Fig. 8) to a contour surrounding the region of singularities in the complex κ-domain. Contrary to Fig. 8, the air has again the conductivity $\sigma_0 = 0$. For $r \to \infty$ each path element gives a contribution decaying exponentially $\sim \exp[-r\,\mathrm{Im}(\kappa)]$. The TM-mode contour can be closed already along the path $\mathrm{Im}(\kappa^2) = -\omega\mu_0\sigma_{\min}$ (see Fig. 8) and, therefore, the TM-mode is a superpostion of contributions with a strict exponential decay. The critical point $\kappa = 0$ contributes only to the TE-mode, where the resulting algebraic decay in powers of $1/r$ forms the airwave.

The alternative definition (43) of the complete airwave E_{1r} is based on Q_e^{odd}, which in the context of complex wavenumbers is defined as $Q_e^{\mathrm{odd}}(\kappa) = [Q_e(\sqrt{\kappa^2}) - Q_e(-\sqrt{\kappa^2})]/2$, where $Q_e(-\sqrt{\kappa^2})$ is the image of $Q_e(\sqrt{\kappa^2})$ mirrored at the positive imaginary axis. $Q_e^{\mathrm{odd}}(\kappa)$ is an odd function of $\sqrt{\kappa^2}$. When performing the integral in the definition (43) of E_{1r} in the complex plane, the contribution E_{2r} is obtained from the branch $\mathrm{Im}(\kappa^2) = 0$ plus exponentially decaying fields from integrating $Q_e^{\mathrm{odd}}(\kappa)$ along the terminating branch cut (see Fig. 8). In addition there are exponentially decaying contributions from the TE-mode poles. Whereas E_{2r} is the purest representative of the guided airwave in the range $r > 0$, the airwave E_{1r} in addition contains exponentially decaying fields generated by interaction with the interface $z = 0$. This is clearly demonstrated by the uniform half-space example of Section 3.3.2. The mixed airwave E_{1r}, given in eq. (53), is decomposed via eq. (56) into the pure airwave E_{2r}, given in eq. (54), resulting from the airwave branch, and the exponentially decaying difference eq. (57), resulting from the integration of eq. (50) along the two banks of the terminating branch from ik to $+i\infty$. A further discussion has already been given at the end of Section 3.3.1. See also Fig. 7.

4.3 The resistive-layer mode

A second type of guided waves occurs, if there exists a resistive layer of conductivity σ_r in between two well conducting layers. The resistive layer serves as 'wave guide' for the TM-mode 'resistive-layer mode' introduced in Section 1. Mathematically, this mode is the residual at the resistive-layer pole κ_r. Under the assumption that σ_r is the smallest conductivity encountered in $z > 0$, the pole κ_r is the TM-mode pole of smallest imaginay part. Its existence close to $ik_{\min}$ is indicated in Fig. 8 and is demonstrated for the standard conductivity model in Fig. 9. In this model, the TM-mode pole κ_r is clearly separated from the other six TM-mode poles belonging to the series eq. (81). When κ_r is found, the resistive-layer mode with the decay length $L_r = 1/\mathrm{Im}(\kappa_r)$ is the residual at κ_r.

The following method for the determination of κ_r has turned out to be very useful. From eq. (71), that is,

$$\overline{D}_m = f_{ma}(z) f_{mb}(z) D_m(z) = W_m(z), \tag{85}$$

then follows that $\kappa = \kappa_r$ is the smallest root of

$$D_m(z, \kappa) = a_m(z, \kappa) + b_m(z, \kappa) = 0, \tag{86}$$

where $z > 0$ is arbitrary. Let the uniform resistive layer of thickness d_r be positioned in $z_u < z < z_d$, $d_r = z_d - z_u$, see Fig. 11. The freedom in the selection of z is exploited by solving eq. (86) for $z = z_u$, because for this choice the resulting equation becomes a quite explicit function in the unknown κ_r. The recursion formula (B23) yields as variation of $b_m(z)$ from bottom to top of the resistive layer,

$$b_m(z_u) = \zeta_r \frac{b_m(z_d) + \zeta_r \tanh(\alpha_r d_r)}{\zeta_r + b_m(z_d)\tanh(\alpha_r d_r)}, \tag{87}$$

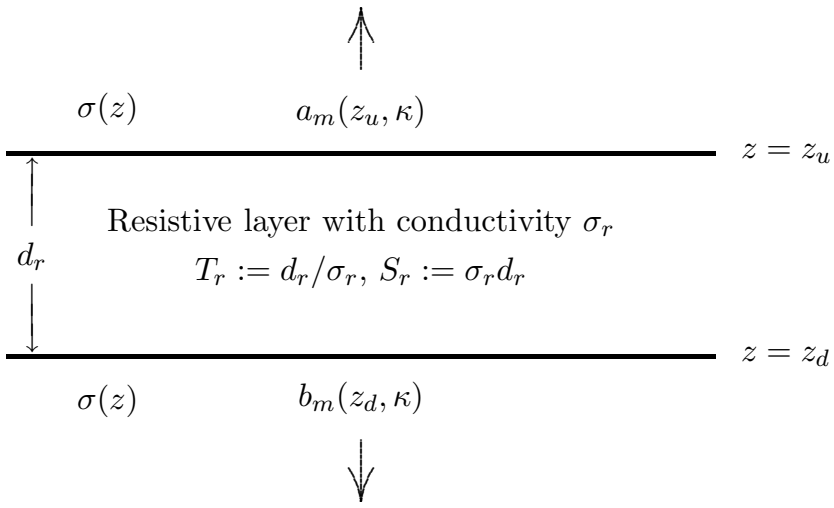

Figure 11. To the computation of the resistive-layer pole κ_r via eq. (90). The functions $a_m(z_u, \kappa)$ and $b_m(z_d, \kappa)$ are the TM-mode spectral impedances for partial waves propagating, respectively, from $z = z_u$ upwards and and from $z = z_d$ downwards.

where $\zeta_r := \alpha_r/\sigma_r$, $\alpha_r^2 := \kappa^2 + k_r^2$, $k_r^2 := i\omega\mu_0\sigma_r$. With the further abbreviations

$$T_r := d_r/\sigma_r, \quad S_r := d_r\sigma_r \text{ and } c := \alpha_r d_r \coth(\alpha_r d_r), \tag{88}$$

a reformulation of eq. (87) yields

$$b_m(z_u) = \frac{c\, b_m(z_d) + \alpha_r^2 T_r}{c + S_r b_m(z_d)}. \tag{89}$$

After inserting this expression into eq. (86) for $z = z_u$ and solving for α_r^2, the implicit equation

$$\kappa^2 = -k_r^2 - \{[a_m(z_u, \kappa) + b_m(z_d, \kappa)]\, c(\kappa) + a_m(z_u, \kappa)\, b_m(z_d, \kappa) S_r\} / T_r \tag{90}$$

is obtained for the determination of $\kappa = \kappa_r$. A simple iterative solution with the starting point $\kappa = 0$ converges after a few iterations, if the integrated resistivity T_r is sufficiently large. Generally an iterative solution of the equation $x = f(x)$ exists, if $f(x)$ is contracting, that is, $|f'(x)| < 1$. After dropping insignificant terms in (90) (see eq. 93), this condition is equivalent to

$$\left| \frac{\partial[a_m(z_u, \kappa) + b_m(z_d, \kappa)]}{\partial \kappa^2} \right| < T_r. \tag{91}$$

In Appendix B3 it is shown that

$$\frac{\partial a_m(z_u, \kappa)}{\partial \kappa^2} = \int_{0+}^{z_u} \frac{f_{ma}^2(t, \kappa)}{f_{ma}^2(z_u, \kappa)} \cdot \frac{\mathrm{d}t}{\sigma(t)} \quad \text{and} \quad \frac{\partial b_m(z_d, \kappa)}{\partial \kappa^2} = \int_{z_d}^{\infty} \frac{f_{mb}^2(t, \kappa)}{f_{mb}^2(z_d, \kappa)} \cdot \frac{\mathrm{d}t}{\sigma(t)}. \tag{92}$$

Eqs (91) and (92) are then interpreted in the sense that the iteration converges, if the integrated resistivity of the resistive layer is greater than the field-weighted integrated resistivity of the conductors outside the layer. The 'standard model' of Fig. 1 requires $T_r > 1000\ \Omega\mathrm{m}^2$. For smaller T_r, nonlinear equation solvers are required.

The spectral impedance $a_m(z_u, \kappa)$ depends only on the conductivity distribution above the resistive layer. Similarly, $b_m(z_d, \kappa)$ depends only on $\sigma(z)$ in $z > z_d$. For an earth consisting of uniform layers, these transfer functions are easily obtained by recursion (see Appendix B4).

The exact formula (90) can be simplified. Because of the small conductance S_r of the resistive layer, the second term in curly brackets can be neglected. Moreover $|\alpha_r d_r| \ll 1$ and, therefore, $c(\kappa) \approx 1$. Hence,

$$\kappa^2 \approx -k_r^2 - [a_m(z_u, \kappa) + b_m(z_d, \kappa)]/\, T_r. \tag{93}$$

This condition follows also directly from eqs (86) and (87) by approximating the latter equation by

$$b_m(z_u) \approx b_m(z_d) + \zeta_r \tanh(\alpha_r d_r) \approx b_m(z_d) + \alpha_r^2 T_r. \tag{94}$$

The application of eq. (90) to the 'standard model' yields

$$\kappa_r = (-2.7887 + i5.8318) \times 10^{-4}\ \mathrm{m}^{-1}, \tag{95}$$

corresponding to a decay length of $L_r = 1/\mathrm{Im}(\kappa_r) = 1714.7$ m. The result obtained by the approximation (93) differs only slightly,

$$\kappa_r \approx (-2.7896 + i5.8321) \times 10^{-4}\,\mathrm{m}^{-1}. \tag{96}$$

At $\kappa = \kappa_r$, the linear independence of f_{ma} and f_{mb} breaks down. This is formally seen from (86), that is, from $a_m(z, \kappa_r) = -b_m(z, \kappa_r)$, which according to (13) is equivalent to $f'_{ma}/f_{ma} = f'_{mb}/f_{mb}$ or $f_{ma} = \gamma f_{mb}$. Since only field ratios are important, $\gamma = 1$ is taken without loss of generality. Therefore, f_{ma} and f_{mb} merge into the eigensolution f_{mr}, vanishing both at $z = 0$ and for $z \to \infty$,

$$f_{ma}(z, \kappa_r) = f_{mb}(z, \kappa_r) =: f_{mr}(z). \tag{97}$$

This eigensolution, with its peak amplitude in the resistive layer, is displayed in Fig. 12.

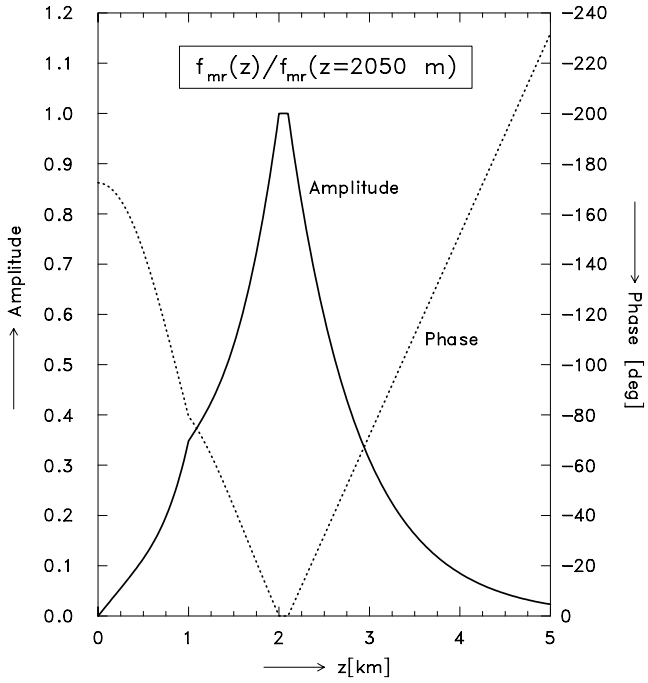

Figure 12. The eigensolution $f_{mr}(z)$ of the resistive-layer mode for the standard conductivity model of Fig. 1. Displayed is $f_{mr}(z)$, normalized with respect to its value in the centre $z = z_r$ of the resistive layer. Here $f_{mr}(z)$ attains its largest amplitude and phase. The exponential variation of $f_{mr}(z)$ in the uniform host below the resistive layer induces a linear phase change. The slope discontinuities at $z = 1$ km mark the seafloor.

The resistive-layer mode (superscript *rlm*) is the residual of the TM-mode at $\kappa = \kappa_r$. From eqs (15), (16), (18), (68), (85), (86) and (97) it follows that

$$E_r^{rlm}(\mathbf{r}) = \epsilon(z\,|\,z_0)\,\partial_r H_1^{(1)}(\kappa_r r)\cos\varphi, \quad E_\varphi^{rlm}(\mathbf{r}) = -[\epsilon(z\,|\,z_0)/r]\,H_1^{(1)}(\kappa_r r)\sin\varphi \tag{98}$$

with

$$\epsilon(z\,|\,z_0) := \frac{ip}{2}\,\frac{a_m(z,\kappa_r)\,a_m(z_0,\kappa_r)\,f_{mr}(z)\,f_{mr}(z_0)}{\partial_\kappa \overline{D}_m(\kappa)|_{\kappa=\kappa_r}}, \tag{99}$$

Then $\epsilon(z|z_0) = \epsilon(z_0|z)$. An alternative formulation is obtained by using the identity $a_m(z,\kappa_r)f_{mr}(z) = f'_{mr}(z)/\sigma(z)$, which follows from eqs (13) and (97). For an actual evaluation, the denominator of eq. (99) is replaced by

$$\partial_\kappa \overline{D}_m(\kappa)|_{\kappa=\kappa_r} = f_{mr}^2(\overline{z})\,\partial_\kappa D_m(\overline{z},\kappa)|_{\kappa=\kappa_r}, \tag{100}$$

where eqs (85) and (86) have been used. The depth $\overline{z} > 0$ is arbitrary, for example, $\overline{z} = z$ or $\overline{z} = z_0$. The κ-derivative on the right-hand side of eq. (100) is readily determined numerically. Nevertheless, a useful approximation of the derivative can be derived from the exact integral representation

$$\partial_\kappa D_m(\overline{z},\kappa)|_{\kappa=\kappa_r} = 2\kappa_r \int_{0^+}^{\infty} \frac{f_{mr}^2(t)}{f_{mr}^2(\overline{z})}\cdot\frac{\mathrm{d}t}{\sigma(t)}, \tag{101}$$

easily deduced from eq. (92) with $z_d = z_u = \overline{z}$ and the linear dependence (97). The main contribution to the integral comes from the resistive layer, where both $1/\sigma$ and the amplitude of $f_{mr}(z)$ are large (see Fig. 12). Thus eqs (100) and (101) yield

$$\partial_\kappa \overline{D}_m(\kappa)|_{\kappa=\kappa_r} = 2\kappa_r \int_{0^+}^{\infty} f_{mr}^2(t)\cdot\frac{\mathrm{d}t}{\sigma(t)} \approx 2\kappa_r T_r f_{mr}^2(z_r), \tag{102}$$

where z_r is depth to the centre of the resistive layer. Therefore, eq. (99) is approximated by

$$\epsilon(z\,|\,z_0) \approx \frac{ip}{4}\,\frac{a_m(z,\kappa_r)\,a_m(z_0,\kappa_r)\,f_{mr}(z)\,f_{mr}(z_0)}{\kappa_r T_r f_{mr}^2(z_r)}. \tag{103}$$

For the 'standard model' (Fig. 1), the error of the approximation eq. (102) is 3.5 per cent.

Fig. 13 illustrates for this model that the remainder after subtracting the complete airwave (dotted) agrees in the far-field with the resistive-layer mode predicted by eqs (98) and (99). Therefore, in the 'standard model', the airwave branch and resistive-layer pole together give an excellent description of the electric field over a wide range of separations. Fig. 13 also shows as a dash-dotted line the component E_r, without the airwave, for the case where the poorly conducting target layer is replaced by the host conductivity. In this situation a resistive-layer pole no longer occurs and the asymptotic exponential behaviour is controlled by the TM-mode singularity with the smallest imaginary part. This singularity turns out to be the branch point $ik_t = (-1+i)\sqrt{\omega\mu_0\sigma_t/2}$ with $\sigma_t = 1\ \mathrm{S\,m^{-1}}$, see Fig. 8. Therefore, the decay is skin-effect controlled with the decay length $1/\mathrm{Im}(ik_t) \approx 700$ m, whereas the TM-mode pole with the smallest imaginary part is associated with a decay length of only 300 m.

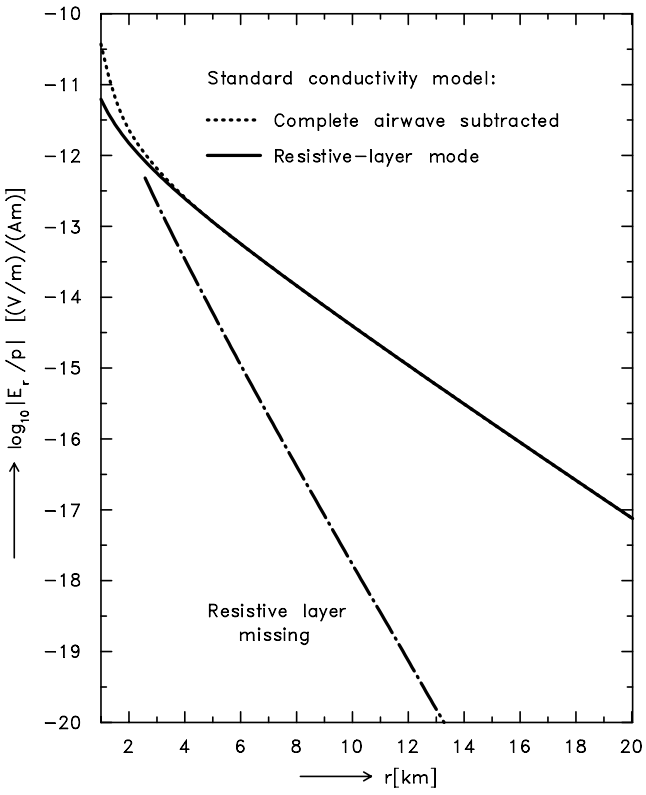

Figure 13. Standard conductivity model of Fig. 1 with $d_1 = z = z_0 = 1000$ m and $f = 0.5$ Hz: the solid line represents the resistive-layer mode eq. (98), which in the far-field ($r > 4$ km) is in full agreement with the remainder after subtracting the complete airwave eq. (44), dotted line. In the linear r-scale, the asymptotic exponential character is evident. The resulting decay length $L \approx 1700$ m is longer than the skin-effect controlled decay length $L \approx 700$ m of a model, where the resistive layer is replaced by a 1 S m^{-1} conductive layer (dot–dashed line, complete airwave removed).

Finally, consider the vertical component $E_z^{rlm}(\mathbf{r})$. In view of $E_z^{\text{air}}(\mathbf{r}) = 0$, the resistive-layer mode dominates the far-field. From eqs (5), (8) and (9) follows

$$E_z^{rlm}(\mathbf{r}) = \epsilon_z(z \mid z_0)\, H_1^{(1)}(\kappa_r r) \cos\varphi \tag{104}$$

with

$$\epsilon_z(z \mid z_0) := \frac{ip}{2\sigma(z)} \frac{\kappa_r^2 a_m(z_0, \kappa_r) f_{mr}(z) f_{mr}(z_0)}{\partial_\kappa \overline{D}_m(\kappa)|_{\kappa=\kappa_r}}, \tag{105}$$

or with the approximation eq. (102),

$$\epsilon_z(z \mid z_0) \approx \frac{ip}{4\sigma(z)} \frac{\kappa_r a_m(z_0, \kappa_r) f_{mr}(z) f_{mr}(z_0)}{T_r f_{mr}^2(z_r)}. \tag{106}$$

As a consequence of the asymptotic behaviour (66), all components of $\mathbf{E}^{rlm}(\mathbf{r})$ decay for $r \to \infty$ exponentially $\sim \exp[-\text{Im}(\kappa_r) r] = \exp(-r/L_r)$. Since E_z is not affected by the airwave, a reliable measurement of this component would have useful discrimination capabilities (see Fig. 5).

5 CONCLUSIONS

With restriction to HED sources and frequency domain electric field data, this study gives an account of the two relevant guided waves in marine CSEM, the airwave and the resistive-layer mode. In view of the renewed interest in the subject, most of the results might already be known, but are buried in technical reports. The emphasis in this study lies more on fundamental principles rather than on practical considerations. Therefore, the results are illustrated by a single 'standard model' only, rather than by a variety of models.

The two waves are complementary. The airwave, guided along the air–ocean interface, is a TE-mode phenomenon that decays in powers of $1/r$, the resistive-layer mode, guided in the thin reservoir layer, is a TM-mode phenomenon with an exponential decay. With respect to the information contents, the airwave is unwanted noise, the resistive-layer mode useful signal.

We did not address the practically important problem of removing the airwave. Subtraction of the airwave in Figs 4 and 6 is done under the assumption that the underlying conductivity structurewe is exactly known. Nevertheless, the results allow some general conclusions. Since the conductivity parameters in CSEM do not vary widely, a reliable guess can be made for $\sigma(z)$, including other sources of information such

as water depth, water conductivity and borehole logs. On this basis, the leading term of the airwave is easily estimated using eqs (22)–(24). Moreover, the leading term turns out to be virtually independent of the parameters of the resistive layer.

The airwave is present in five of the six electromagnetic field components. Only E_z, which is a pure TM-mode, is not affected by the airwave and shows an exponential decay dominated by the resistive-layer mode. Therefore, a reliable measurement of this component would be of importance for hydrocarbon exploration in a shallow sea.

In Section 4, we have made an effort to interpret the radial decay of electric fields in terms of singularities of the electric field kernels Q_e and Q_m in the complex wavenumber domain. Viewed from this perspective, it was possible to identify and isolate a 'pure' complete airwave as the branch-cut integral of TE-mode kernels along the positive imaginary axis and the resistive-layer mode as the residual of the TM-mode pole with the smallest imaginary part. This study concludes with the remarkable result that in case of the 'standard model' the superposition of only these two guided waves yields an excellent description of the electric field over a wide range of separations.

ACKNOWLEDGMENTS

I am indebted to the editor Tim Minshull and to the reviewers Katrin Schwalenberg and Rob Evans for their thoughtful criticism, which (hopefully) has improved the readability of the paper. My particular thanks go to Randy Mackie, who at the beginning has challenged this study and at the end has improved the manuscript by a bunch of very helpful suggestions.

REFERENCES

Abramowitz, M. & Stegun, I.A., 1972. *Handbook of Mathematical Functions*, Dover Publications, Inc., New York.

Bannister, P.R., 1984. New simplified formulas for ELF subsurface to subsurface propagation, *IEEE J. Ocean. Eng.,* **9,** 154–163.

Chave, A.D. & Cox, C.S., 1982. Controlled electromagnetic sources for measuring the electrical conductivity beneath the oceans, *J. geophys. Res,* **87,** 5327–5338.

Chave, A.D., Constable, S. C. & Edwards, R.N., 1991. Electrical exploration methods for the seafloor, in *Electromagnetic Methods in Applied Geophysics,* Vol. 2, pp. 931–966, ed. Nabighian, M.N., Society of Exploration Geophysicists, Tulsa.

Chew, W.C., 1995. *Waves and Fields in Inhomogeneous Media*, IEEE Press, Piscataway, New Jersey.

Constable, S.C. & Weiss, C.J., 2006. Mapping thin resistors and hydrocarbons with marine EM methods: insights from 1D modeling, *Geophysics,* **71,** G43–G51.

Cox, C.S., 1980. Electromagnetic induction in the oceans and inferences on the constitution of the earth, *Geophys. Surv.,* **4,** 137–156.

Edwards, N., 2005. Marine controlled source electromagnetics: principles, methodologies, future commercial applications, *Surv. Geophys.,* **26,** 675–700.

Eidsmo, T., Ellingsrud, S., MacGregor, L.M., Constable, S., Sinha, M.C., Johanson, S., Kong, F.N. & Westerdahl, H., 2002. Sea Bed Logging (SBL), a new method for remote and direct identification of hydrocarbon filled layers in deepwater areas, *First Break,* **20,** 144–152.

Ellingsrud, S., Eidsmo, T., Johanson, S., Sinha, M.C., MacGregor, L.M. & Constable, S., 2002. Remote sensing of hydrocarbon layers by seabed logging (SBL): results from a cruise offshore Angola, *The Leading Edge,* **21,** 972–982.

Goldman, M.M., 1990. *Non-Conventional Methods in Geoelectrical Prospecting*, Ellis Horwood Series in Applied Geology, Ellis Horwood Ltd., New York.

Gradshteyn, I.S. & Ryzhik, I.M., 1980. *Table of Integrals, Series and Products*, Academic Press, New York.

Jackson, J.D., 1975. *Classical Electrodynamics*, John Wiley & Sons Inc., New York.

Jones, D.S., 1964. *The Theory of Electromagnetism*, Pergamon Press, Oxford.

Kaufman, A.A. & Keller, G.V., 1983. Frequency and transient sounding, in *Methods in Geochemistry and Geophysics,* Vol. 16, Elsevier, Amsterdam.

King, R.W.P., Owens, M. & Wu, T.T., 1992. *Lateral Electromagnetic Waves*, Springer-Verlag, New York.

Løseth, L.O., Pedersen, H.M., Ursin, B., Amundsen, L. & Ellingsrud, S., 2006. Low-frequency electromagnetic fields in applied geophysics: waves or diffusion? *Geophysics,* **71,** W29–W40.

Stratton, J.A., 1941. *Electromagnetic Theory*, McGraw-Hill Book Company, New York.

Tranter, C.J., 1966. Integral transforms in mathematical physics, in *Methuen's Monographs on Physical Subjects*, Methuen & Co. Ltd., London.

Um, E.S. & Alumbaugh, D.L., 2007. On the physics of the marine controlled-source electromagnetic method, *Geophysics,* **72,** WA13–WA26.

Wait, J.R., 1961. The electromagnetic fields of a horizontal dipole in the presence of a conducting half-space, *Can. J. Phys.,* **39,** 1017–1028.

Ward, S.H. & Hohmann, G.W., 1987. Electromagnetic theory for geophysical applications, in *Electromagnetic Methods in Applied Geophysics—Theory,* Vol. 1, ed. Nabighian, M.N., Society of Exploration Geophysicists, Tulsa, Oklahoma.

APPENDIX A: THE LEADING TERM IN THE AIRWAVE

A1 Proof of eq. (29)

For a proof of eq. (29), that is,

$$Q_e(z \mid z_0, 0) = Q_m(z \mid z_0, 0) \tag{A1}$$

with Q_e and Q_m defined in eqs (17) and (18), $f_e(z, \kappa)$ and $f_m(z, \kappa)$ have to be considered in the limit $\kappa = 0$. Then the differential eqs (10) and (12) read

$$f_e''(z, 0) = i\omega\mu_0\sigma(z) f_e(z, 0), \quad [f_m'(z, 0)/\sigma(z)]' = i\omega\mu_0 f_m(z, 0). \tag{A2}$$

Let $g := f_m'/\sigma$. Then $g' = i\omega\mu_0 f_m$, $g'' = i\omega\mu_0 f_m' = i\omega\mu_0\sigma g$. Therefore, $g(z)$ and $f_e(z, 0)$ satisfy identical differential equations and for $f_m(z, 0) = f_{ma}(z, 0)$ or $f_{mb}(z, 0)$ the function $g(z)$ is a multiple of $f_{ea}(z, 0)$ or $f_{eb}(z, 0)$, that is, $g(z) = \gamma f_{ea,b}(z, 0)$, where γ is a non-zero

constant. Hence, using also eqs (11) and (13), it follows that

$$f'_{ma,b}(z,0) = \gamma\sigma(z) f_{ea,b}(z,0), \quad \gamma f'_{ea,b}(z,0) = i\omega\mu_0 f_{ma,b}(z,0), \tag{A3}$$

$$a_m(z,0) = i\omega\mu_0/a_e(z,0), \quad b_m(z,0) = i\omega\mu_0/b_e(z,0). \tag{A4}$$

Using these equations, the TM-mode quantities can be replaced by the TE-mode quantities in $Q_m(z|z_0,0)$, see eq. (18). Let for example $z \geq z_0$. Then from eqs (17), (18) and (11) it is deduced, after a little algebra, that

$$Q_m(z\,|\,z_0,0) = \frac{f_{eb}(z,0)/f_{eb}(z_0,0)}{a_e(z_0,0)+b_e(z_0,0)} = Q_e(z\,|\,z_0,0). \tag{A5}$$

This proves eq. (29) = (A1). The physical interpretation of eqs (A3) and (A4) is that the horizontally uniform electric and magnetic fields resulting from $\kappa = 0$ can be associated either with a TE-mode (large horizontal current loops) or with a TM-mode (large vertical current loops). In particular, eq. (A4) expresses the fact that in this case TE- and TM-mode impedance agree.

A2 Proof of eq. (30)

In this Appendix, we prove the relations (30), that is,

$$Q_e(z\,|\,z_0,-\kappa) \neq Q_e(z\,|\,z_0,+\kappa), \quad Q_m(z\,|\,z_0,-\kappa) = Q_m(z\,|\,z_0,+\kappa). \tag{A6}$$

For simplicity it is assumed that in $z > 0$ the conductivity $\sigma(z)$ is bounded from below by $\sigma_{\min}$, $\sigma(z) \geq \sigma_{\min} > 0$. Moreover, it is assumed that $\sigma(z)$ terminates with a constant conductivity $\sigma_t > 0$ for $z > z_t$, where z_t is a great depth. Recalling that $\alpha^2 = \kappa^2 + i\omega\mu_0\sigma$, the following results are obtained:

(1) $b_e(z,\kappa)$ is an even function of κ:
From eqs (10) and (11) it follows that $b_e(z,\kappa)$ solves the Riccati equation

$$b'_e(z,\kappa) = -b_e^2(z,\kappa) + \alpha^2(z,\kappa). \tag{A7}$$

The solution $f_e(z) \sim \exp(-\alpha_t z)$ for $z \geq z_t$, $\alpha_t^2 := \kappa^2 + i\omega\mu_0\sigma_t$, implies that $b_e(z_t,\kappa) = \alpha_t(\kappa)$. When integrating eq. (A7) with this initial value from $z = z_t$ upwards, it is seen that $b_e(z,\kappa)$, $z \geq 0$, is an even function of κ.

(2) $a_e(z,\kappa)$ has an even and an odd part:
From eqs (10) and (11) it follows that $a_e(z,\kappa)$ solves the Riccati equation

$$a'_e(z,\kappa) = a_e^2(z,\kappa) - \alpha^2(z,\kappa). \tag{A8}$$

Observing the continuity of $f_{ea}(z)$ and $f'_{ea}(z)$ at $z = 0$, the solution $f_{ea}(z) \sim \exp(\kappa z)$ for $z < 0$ implies that $a_e(0,\kappa) = \kappa$. When integrating eq. (A8) with this initial value from $z = 0$ downwards, it is seen that $a_e(z,\kappa)$, $z > 0$, has both an even and an odd part.

(3) $b_m(z,\kappa)$ is an even function of κ:
From eqs (12) and (13) it follows that $b_m(z,\kappa)$ solves the Riccati equation

$$b'_m(z,\kappa) = -\sigma(z) b_m^2(z,\kappa) + \alpha^2(z,\kappa)/\sigma(z). \tag{A9}$$

Similarly as in the case $b_e(z,\kappa)$, an upward integration of eq. (A9) with the initial value $b_m(z_t,\kappa) = \alpha_t(\kappa)/\sigma_t$ qualifies $b_m(z,\kappa)$ as an even function of κ.

(4) $a_m(z,\kappa)$ is an even function of κ:
A vanishing vertical current density $J_z = \sigma E_z = -(1/\mu_0)(\partial_{xx}^2 + \partial_{yy}^2)\,\chi_m$ (see eq. 5) at $z = 0$ requires $f_{ma}(0,\kappa) = 0$. Therefore, consider the spectral admittance $\overline{a}_m(z,\kappa) := 1/a_m(z,\kappa)$, satisfying according to eqs (12) and (13) the Riccati equation

$$\overline{a}'_m(z,\kappa) = \sigma(z) - \overline{a}_m^2(z,\kappa)\alpha^2(z,\kappa)/\sigma(z) \tag{A10}$$

with the initial value $\overline{a}_m(0^+,\kappa) = 0$. Downward integration of eq. (A10) then shows that $\overline{a}_m(z,\kappa)$ [and $a_m(z,\kappa)$] is an even function of κ.

On using eqs (11) and (13), the symmetry in the transfer functions is mapped onto the field ratios via

$$\frac{f_{eb}(z,\kappa)}{f_{eb}(z_0,\kappa)} = \exp\left[-\int_{z_0}^{z} b_e(t,\kappa)\,\mathrm{d}t\right], \quad \frac{f_{mb}(z,\kappa)}{f_{mb}(z_0,\kappa)} = \exp\left[-\int_{z_0}^{z} \sigma(t)\, b_m(t,\kappa)\,\mathrm{d}t\right]. \tag{A11}$$

Corresponding relations apply for f_{ea} and f_{ma}. In conjunction with the definitions (17) and (18) this proves the assertions (30) = (A6).

A3 Evaluation of $\partial_\kappa Q_e(z\,|\,z_0,\kappa)|_{\kappa=0}$

This quantity, which controls the amplitude of the airwave, is required in eqs (31) and (32). For brevity we use the notation

$$\dot{h} := \partial_\kappa h(\kappa)|_{\kappa=0}. \tag{A12}$$

Since Q_m is an even function of κ, implying $\dot{Q}_m = 0$, only $\dot{Q}_e$ contributes in eqs (31) and (32) to the leading term. The reciprocity (19) allows confining attention to $z \geq z_0$. Since $\dot{b}_e = 0$, the only contribution to $\dot{Q}_e$ comes from a_e in the denominator of eq. (17). To compute $\dot{a}_e(z)$, we first deduce, from eq. (10) by differentiation with respect to κ and subsequently putting $\kappa = 0$, that $\dot{f}_{ea}(z)$ satisfies the differential equation

$$\dot{f}''_{ea}(z) = i\omega\mu_0\sigma(z)\dot{f}_{ea}(z), \tag{A13}$$

which coincides with eq. (10) for $\kappa = 0$. Therefore, the corresponding Wronskian is independent of z,

$$\overline{W}_{ea}(z) := f_{ea}(z,0)\dot{f}'_{ea}(z) - f'_{ea}(z,0)\,\dot{f}_{ea}(z) = \text{const.} \tag{A14}$$

From $f_{ea}(z,\kappa) = f_{ea}(0,\kappa)\exp(\kappa z)$ it follows that $\overline{W}_{ea}(0) = f^2_{ea}(0,0)$. For this reason,

$$\dot{a}_e(z) = \overline{W}_{ea}(z)/f^2_{ea}(z,0) = \overline{W}_{ea}(0)/f^2_{ea}(z,0) = f^2_{ea}(0,0)/f^2_{ea}(z,0). \tag{A15}$$

Now $\dot{Q}_e(z\,|\,z_0)$ can be evaluated. Eqs (17), (A15) and (20) yield

$$\begin{aligned}\dot{Q}_e(z\,|\,z_0) &= -\frac{\dot{a}_e(z_0)\,f_{eb}(z,0)/f_{eb}(z_0,0)}{[a_e(z_0,0)+b_e(z_0,0)]^2} = -\frac{f^2_{ea}(0,0)\,f_{eb}(z,0)\,f_{eb}(z_0,0)}{W^2_e(z_0)}\\ &= -\frac{f^2_{ea}(0,0)\,f_{eb}(z,0)\,f_{eb}(z_0,0)}{W^2_e(0)} = -\frac{f_{eb}(z,0)\,f_{eb}(z_0,0)}{[f'_{eb}(0,0)]^2}.\end{aligned} \tag{A16}$$

The last step is based on

$$W_e(0) = -f'_{eb}(0,0)\,f_{ea}(0,0), \tag{A17}$$

since $f'_{ea}(0,0) = 0$. By inserting eq. (A16) into eqs (31) and (32) and using the simplified notation $e(z) := f_{eb}(z,0)$, we arrive at the airwave representation (22) and (23).

A4 Sketch of the proof of eq. (34)

The result (34) can be verified as follows. From eq. (5) it is inferred (with ∇^2_h as horizontal projection of the Laplace operator) that

$$E_z(\mathbf{r}) = -\frac{1}{\mu_0\sigma(z)}\nabla^2_h\chi_m(\mathbf{r}), \tag{A18}$$

which according to eq. (9) requires the consideration of $f_{ma}(z)/\sigma(z)$ at $z = 0^-$, where numerator and denominator both vanish, such that the ratio is indefinite. Its value can be determined via the continuity of $f'_{ma}(z)/\sigma(z)$ across the interface. In the air $z < 0$ assume $\sigma(z) = \sigma_0 > 0$ and consider the limit $\sigma_0 \to 0$. Thus in the air–half-space $f_{ma}(z) \sim \exp(\alpha_0 z)$ and $f_{ma}(z) = f'_{ma}(z)/\alpha_0$, $\alpha^2_0 := \kappa^2 + i\omega\mu_0\sigma_0$. Then

$$\lim_{\sigma_0\to 0}\frac{f_{ma}(0^-)}{\sigma_0} = \lim_{\sigma_0\to 0}\frac{f'_{ma}(0^-)}{\alpha_0\sigma_0} = \frac{f'_{ma}(0^+)}{\kappa\sigma(0^+)} \tag{A19}$$

leads to a definite value. With eqs (A19) and (9) it is infered from eq. (A18) that

$$E_z(r,0^-) = -\frac{p\cos\varphi}{2\pi\sigma(0^+)}\int_0^\infty \frac{b_m(z_0)f'_{ma}(0^+)/f_{ma}(z_0)}{a_m(z_0)+b_m(z_0)}\,\kappa\,J_1(\kappa r)\,\mathrm{d}\kappa, \tag{A20}$$

where it was noted that $\nabla^2_h\,[J_1(\kappa r)\cos\varphi] = -\kappa^2 J_1(\kappa r)\cos\varphi$. The asymptotic formula (28) yields as leading term of eq. (A20)

$$E_z(r,0^-) \approx -\frac{p\cos\varphi}{2\pi\sigma(0^+)r^2}\,\frac{b_m(z_0,0)f'_{ma}(0^+,0)/f_{ma}(z_0,0)}{a_m(z_0,0)+b_m(z_0,0)}. \tag{A21}$$

Via eqs (A3) and (A4), the TM-mode is replaced by the TE-mode. After simplifying the result with the Wronskian relations (20) and (A17), the result is eq. (34).

APPENDIX B: TECHNICAL DETAILS

B1 Explicit forms of the complete uniform-half-space airwave

Implicit forms of the uniform-half-space airwave are given in eqs (53), (54) and (57). Performing differentiations with respect to r and z results in

$$E_{1r}(\mathbf{r}) = +\gamma\left[(w^2_+ - w^2_-)(a_0d_0 - a_1d_1) + 2w_+a_0d_1 + 2w_-a_1d_0\right], \tag{B1}$$

$$E_{2r}(\mathbf{r}) = +\gamma\left[(w^2_+ - w^2_-)(b_0d_0 - b_1d_1) + 2w_+b_0d_1 + 2w_-b_1d_0\right], \tag{B2}$$

$$E_{1r}(\mathbf{r}) - E_{2r}(\mathbf{r}) = -\gamma\left[(w^2_+ - w^2_-)(c_0d_0 + c_1d_1) + 2w_+c_0d_1 - 2w_-c_1d_0\right], \tag{B3}$$

where

$$a_n := i\pi I_n(w_-),\ b_n := K_n(\mathrm{e}^{-i\pi}w_-),\ c_n := K_n(w_-),\ d_n := K_n(w_+),\ n = 0,1 \tag{B4}$$

and

$$\gamma := \frac{p\cos\varphi}{4\pi^2 i\sigma R^3_+}. \tag{B5}$$

According to formula 9.6.31 of Abramowitz & Stegun (1972), a_n, b_n and c_n are interrelated by

$$a_n = b_n - (-1)^n c_n. \tag{B6}$$

B2 Asymptotic distribution of TM-mode poles for a simple model

In eq. (81) of Section 4.1, we have given the asymptotic distribution of the TM-mode poles of the standard model. Here a short derivation of this result is presented. Replacing the resistive layer by an insulator, the simplified model consists of the sea with conductivity σ_1, and depth d_1, the sediments with conductivity σ_2 and thickness d_2 and an insulator below. According to eq. (80) the required poles are the poles of the surface impedance $b_m(0, \kappa)$. From eq. (B23) it follows that with $b_3 = \infty$, $b_2 = \zeta_2 \coth(\alpha_2 d_2)$ as surface impedance

$$b_m(0, \kappa) =: b_1 = \zeta_1 \frac{\zeta_2 \coth(\alpha_2 d_2) + \zeta_1 \tanh(\alpha_1 d_1)}{\zeta_1 + \zeta_2 \coth(\alpha_2 d_2) \tanh(\alpha_1 d_1)}, \tag{B7}$$

which provides the pole condition

$$\zeta_1 \cosh(\alpha_1 d_1) \sinh(\alpha_2 d_2) + \zeta_2 \cosh(\alpha_2 d_2) \sinh(\alpha_1 d_1) = 0, \tag{B8}$$

or equivalently

$$(\zeta_1 + \zeta_2) \sinh(\alpha_1 d_1 + \alpha_2 d_2) + (\zeta_1 - \zeta_2) \sinh(\alpha_2 d_2 - \alpha_1 d_1) = 0, \tag{B9}$$

where $\alpha_j^2 = \kappa^2 + i\omega\mu_0\sigma_j$, $\zeta_j = \alpha_j/\sigma_j$. For $\sigma_1 = \sigma_2 =: \sigma$, implying $\alpha_1 = \alpha_2 =: \alpha$, $\zeta_1 = \zeta_2$, condition (B9) simplifies to $\sinh(\alpha D) = 0$, $D := d_1 + d_2$, or

$$\kappa_n^2 = -(n\pi/D)^2 - i\omega\mu_0\sigma, \quad n = 0, 1, 2, \ldots \tag{B10}$$

Guided by condition (B10), we try as squared pole positions

$$\kappa_n^2 = -(n\pi/D)^2 - i\omega\mu_0\epsilon_n. \tag{B11}$$

Assuming that ϵ_n increases with n slower than n^2, α_j is for $n \gg 1$ approximated by

$$\alpha_j \approx in\pi/D + \omega\mu_0 D(\sigma_j - \epsilon_n)/(2n\pi). \tag{B12}$$

When inserting the resulting expressions for α_j and $\zeta_j = \alpha_j/\sigma_j$ into condition (B9), it is taken into account that $\sinh(\alpha_1 d_1 + \alpha_2 d_2) = \sinh(in\pi + \gamma) = (-1)^n \sinh\gamma \approx (-1)^n\gamma$, where

$$\gamma := \omega\mu_0 D(\sigma_1 d_1 + \sigma_2 d_2 - D\epsilon_n)/(2n\pi). \tag{B13}$$

First we consider the simple case $d_1 = d_2 = D/2$, appropriate for the standard model. Then for $n \to \infty$ the left-hand side of eq. (B9) is $\mathcal{O}(1)$. This leading order vanishes, if

$$(-1)^n(\sigma_1 + \sigma_2)(\sigma_1 + \sigma_2 - 2\epsilon_n) + (\sigma_2 - \sigma_1)^2 = 0, \tag{B14}$$

which implies

$$\epsilon_n = \frac{2\sigma_1\sigma_2}{\sigma_1 + \sigma_2} \text{ for } n \text{ odd} \qquad \text{and} \qquad \epsilon_n = \frac{\sigma_1^2 + \sigma_2^2}{\sigma_1 + \sigma_2} \text{ for } n \text{ even}, \tag{B15}$$

asymptotically valid for $n \gg 1$. In combination with eq. (B11) the approximation eq. (81) is recovered.

When the restriction $d_1 = d_2$ is dropped, the resulting pole structure is less regular, yielding for $n \gg 1$

$$\epsilon_n = (A_n + B_n)/C_n \tag{B16}$$

with

$$A_n := (-1)^n(\sigma_1 + \sigma_2)(\sigma_1 d_1 + \sigma_2 d_2)/D + \cos\beta_n\,(\sigma_2 - \sigma_1)(\sigma_2 d_2 - \sigma_1 d_1)/D \tag{B17}$$

$$B_n := -2n\pi(\sigma_2 - \sigma_1)\sin\beta_n/(i\omega\mu_0 D^2) \tag{B18}$$

$$C_n := (-1)^n(\sigma_1 + \sigma_2) + \cos\beta_n\,(\sigma_2 - \sigma_1)(d_2 - d_1)/D \tag{B19}$$

and $\beta_n := n\pi(d_2 - d_1)/D$.

B3 Proof of eq. (92)

Because of the similarity of the two parts of eq. (92), attention can be confined to the proof of the first part. Let $g_{ma}(z, \kappa) := \partial f_{ma}(z, \kappa)/\partial\kappa^2$. From the TM-mode eq. (12) follows

$$\sigma[f'_{ma}/\sigma]' = \alpha^2 f_{ma}, \tag{B20}$$

$$\sigma[g'_{ma}/\sigma]' = \alpha^2 g_{ma} + f_{ma}. \tag{B21}$$

Now multiply (B21) by f_{ma}/σ and (B20) by g_{ma}/σ and integrate the difference over z from $z = 0^+$ to $z = z_u$. Then integration by parts yields, on using the the insulating half-space boundary conditions $f_{ma}(0, \kappa) = g_{ma}(0, \kappa) = 0$,

$$\frac{f_{ma}(z_u)\,g'_{ma}(z_u) - f'_{ma}(z_u)\,g_{ma}(z_u)}{\sigma(z_u)} = \int_{0^+}^{z_u} f_{ma}^2(z) \cdot \frac{dz}{\sigma(z)}. \tag{B22}$$

From (13) it follows that the left-hand side equals $f_{ma}^2(z_u)\,\partial a_m(z_u, \kappa)/\partial\kappa^2$. In conjunction with (B22), the first part of assertion (92) is verified.

B4 TM-impedances for a layered earth

The solution of (90) for the resistive-layer pole κ_r requires the downgoing TM-mode impedance $b_m(z_d)$ at the bottom of the resistive layer and the upgoing impedance $a_m(z_u)$ at the top of this layer. For an earth consisting of uniform layers, these impedances are easily obtained by recursion (e.g. Ward & Hohmann 1987, p. 206). Consider an N-layered earth consisting of $N-1$ layers with conductivities σ_n and thicknesses d_n and a terminating half-space of conductivity σ_n and let $n = r$, $2 \le r \le N-1$, be the resistive layer. With $\zeta_n := \alpha_n/\sigma_n$, $\alpha_n^2 := \kappa^2 + i\omega\mu_0\sigma_n$ the recursion (see also eq. 87)

$$b_n = \zeta_n \frac{b_{n+1} + \zeta_n \tanh(\alpha_n d_n)}{\zeta_n + b_{n+1}\tanh(\alpha_n d_n)}, \quad n = N-1, \ldots, r+1 \tag{B23}$$

starting with $b_N = \zeta_N$ and the recursion

$$a_{n+1} = \zeta_n \frac{a_n + \zeta_n \tanh(\alpha_n d_n)}{\zeta_n + a_n\tanh(\alpha_n d_n)}, \quad n = 1, \ldots, r-1 \tag{B24}$$

starting with $a_1 = \infty$, yield $b_m(z_d) = b_{r+1}$ and $a_m(z_u) = a_r$.